2. Properties of Graphene

Overview of Graphene

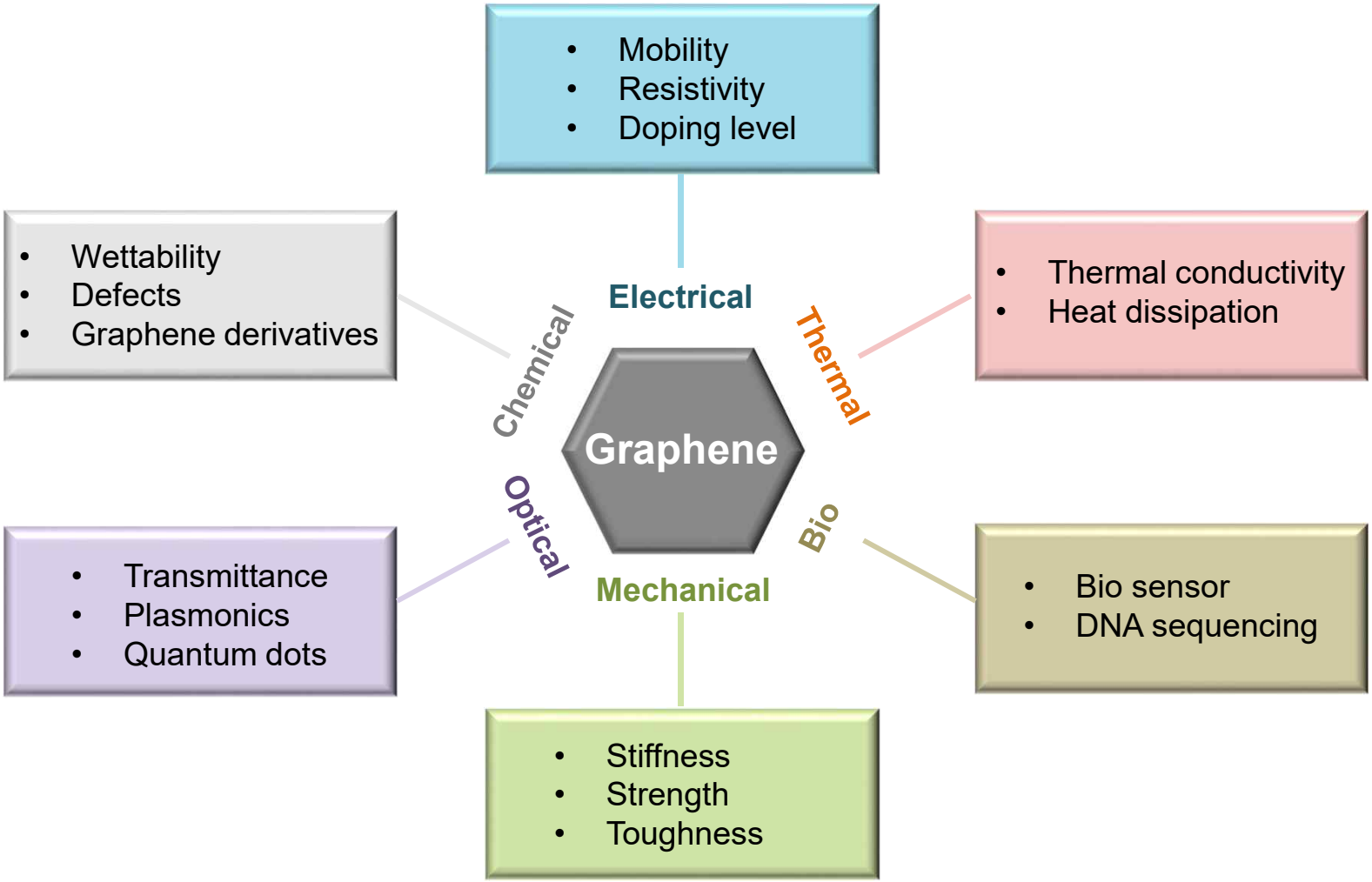

Properties of Graphene

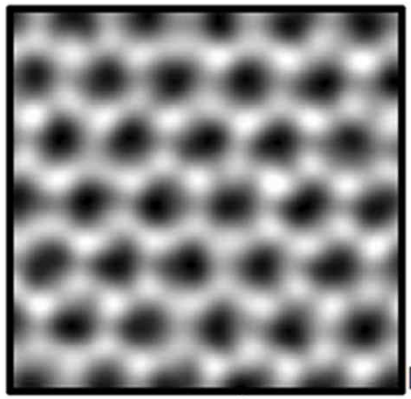

[a]

Exceptional Properties:

- Zero-bandgap Semiconductor with mobility up to 120,000 $cm^2/V\text{-}s$ at RT [b]
- Low Mass
- Stiff: Young's modulus = 1TPa
- Strong: elastic strain of 25 %

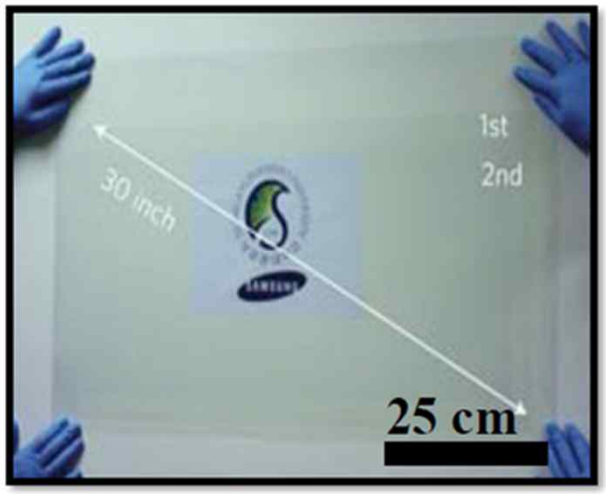

[c]

Ease of Integration:

- Wafer-scale CVD graphene quality equivalent to pristine [c - e]
- CMOS-friendly transfer techniques available

[a] P.Y. Huang, et al., Nature, 2011
[b] K.I. Bolotin, et al., Solid State Communications, 2008
[c] S. Bae, et al., Nature Nano, 2010
[d] G. Lee, et al., Submitted, 2013
[e] N. Petrone, et al., Nano Letters, 2012

Electronic Structure of Graphene

Crystal structure of graphene

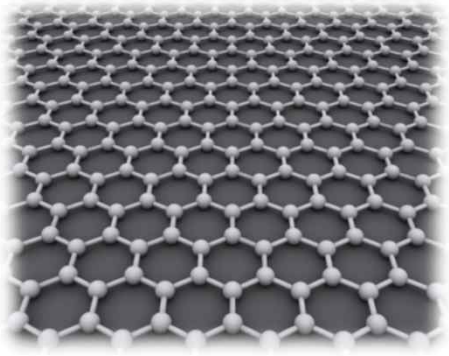

Band structure of graphene

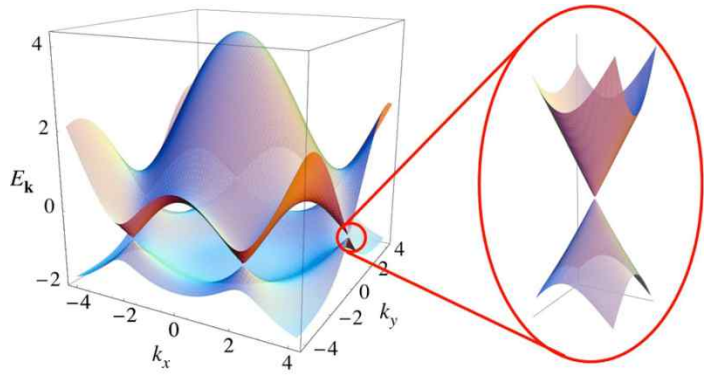

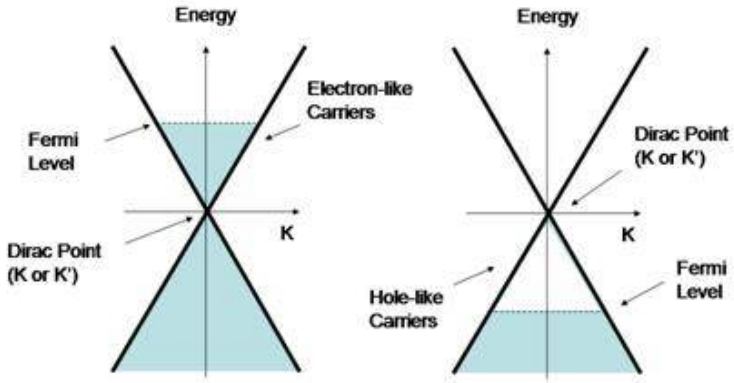

Linear dispersion

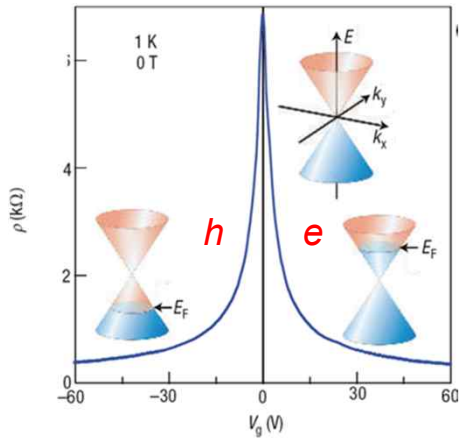

Ambipolar conductance

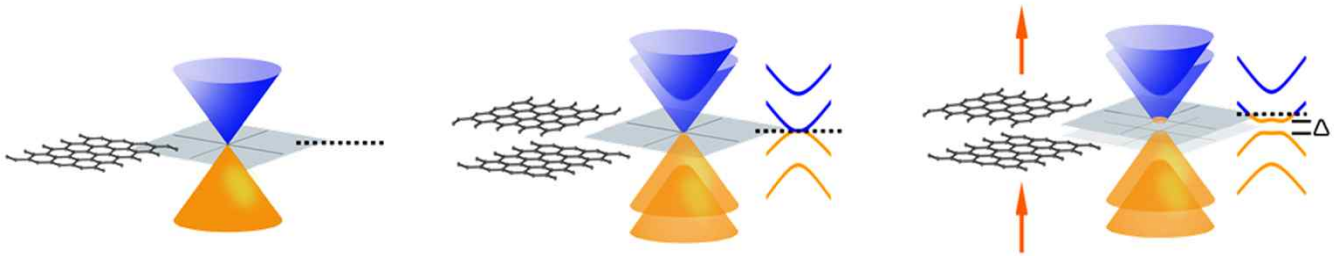

Bandgap opening in bilayer graphene

Electrical Transport in Graphene

Carrier mobility
15,000 $cm^2V^{-1}s^{-1}$ to 200,000 $cm^2V^{-1}s^{-1}$
at a carrier density of 10^{12} cm^{-2} and at room temperature

Resistivity
10^{-6} Ω•cm (< resistivity of silver)

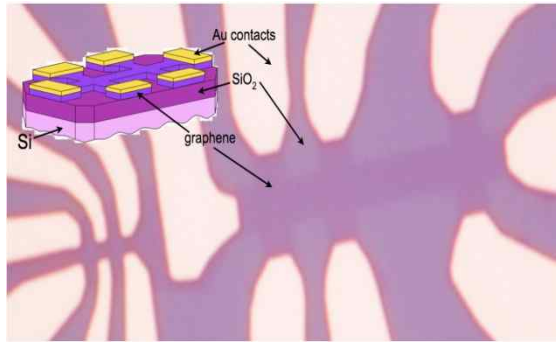

Measurement of carrier mobility

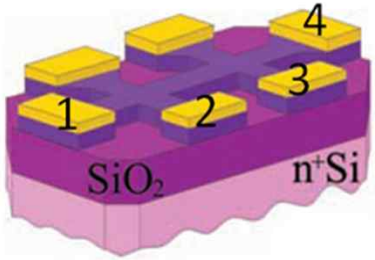

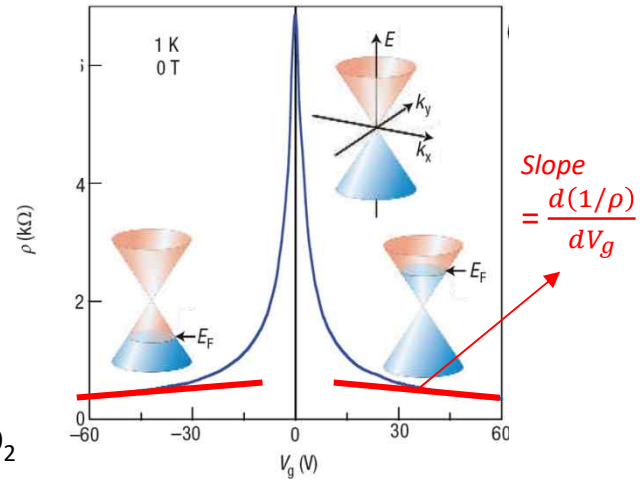

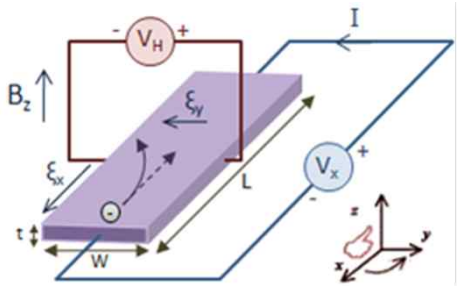

① V_g induces surface charge density (n)

$$n = \frac{\epsilon_0 \epsilon V_g}{te}$$

$\epsilon_0\epsilon$: permittivity of SiO_2
t : thickness of SiO_2
e : electron charge

$$\rho = \frac{W}{L}\frac{V_{23}}{I_{14}}$$

$$\mu = \frac{1}{ne\rho}$$ at specific n

② Field effect mobility

$$\mu_{FE} = \frac{1}{C}\frac{d\sigma}{dV_g} = \frac{1}{C}\frac{d(1/\rho)}{dV_g}$$

③ Hall mobility

$$V_H = \frac{IB}{net}$$

Hall coefficient $(R_H) = \frac{1}{ne}$

$$\mu_{Hall} = \frac{1}{ne\rho} = \frac{R_H}{\rho}$$

A. K. Geim and K. S. Novoselov. Nature Mater. (2007)
J.H. Chen, et al. Nature Nanotechnol. (2008)

Hal bar and error

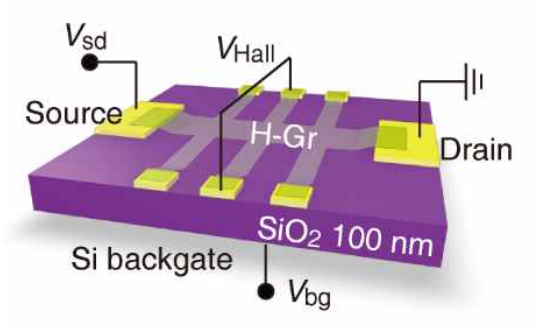

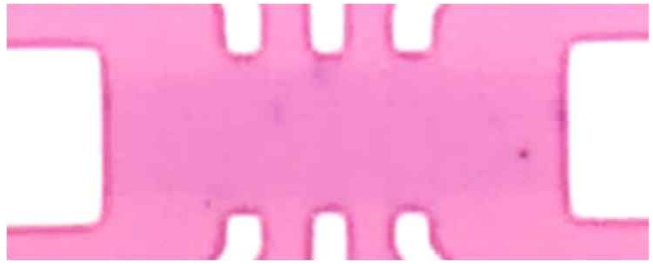

Geometrical error sources in the Hall bar arrangement are caused by deviations of the actual measurement geometry from the ideal of a rectangular solid with constant current density and point-like voltage contacts.

The first geometrical consideration with the Hall bar is the tendency of the end contacts to short out the Hall voltage. If the aspect ratio of sample length to width $l/w = 3$, then this error is less than 1%.[15] Therefore, it's important $l / w \geq 3$.

The finite size of the contacts affects both the current density and electric potential in their vicinity, and may lead to fairly large errors. The errors are larger for a simple rectangular Hall bar than for one in which the contacts are placed at the end of arms.

For a simple rectangle, the error in the Hall mobility can be approximated (when μB << 1) by[16]

$$\frac{\Delta\mu_H}{\mu_H} = 1-(1-e^{-\pi l/2w})(1-2c/\pi w).$$

Here, $\Delta\mu_H$ is the amount μ_H must *increase* to obtain a true value.

If $l/w = 3$, and $c/w = 0.2$, then $\Delta\mu_H / \mu_H = 0.13$, which is certainly a significant error.

Reduce the contact-size error to acceptable levels by placing contacts at the ends of contact arms.[17] The following aspect ratios yield small deviations from the ideal: $p \approx c, c \leq w/3, l \geq 4w$

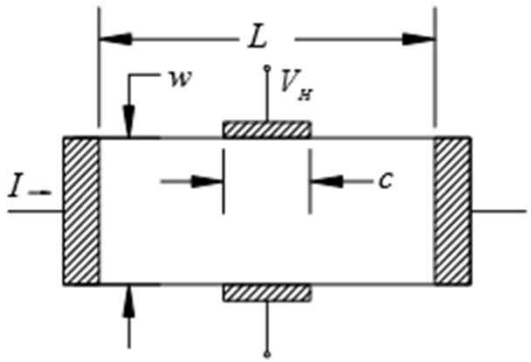

Figure A-7 Hall Bar
With Finite Voltage Contacts

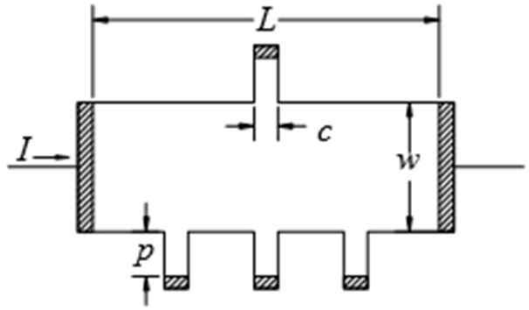

Figure A-8 Hall Bar With Contact Arms

electrical resistivity (ρ)

$$\rho = R\frac{A}{\ell},$$

Resistivity (ρ) has SI units of Ω·m or Ω·cm.

R : electrical resistance of a uniform specimen of the material (measured in Ω)
l : length of the piece of material (measured in m)
A : cross-sectional area of the specimen (measured in m^2).

Conductivity (σ)

$$\sigma = \frac{1}{\rho}.$$

Conductivity has SI units of S/m.

Sheet resistance (R_s)

$$R = \rho\frac{L}{A} = \rho\frac{L}{Wt}$$

$$R = \frac{\rho}{t}\frac{L}{W} = R_s\frac{L}{W}$$

$$\rho = R_s \cdot t$$

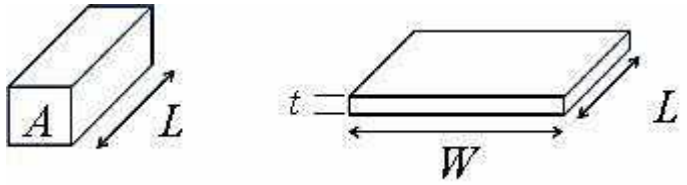

If the film thickness is known, the bulk resistivity (in Ω·cm) can be calculated by multiplying the sheet resistance by the film thickness in cm. Sheet resistance has SI units of $\Omega/\square = \Omega$.

Fundamentals of 2D field-effect transistors

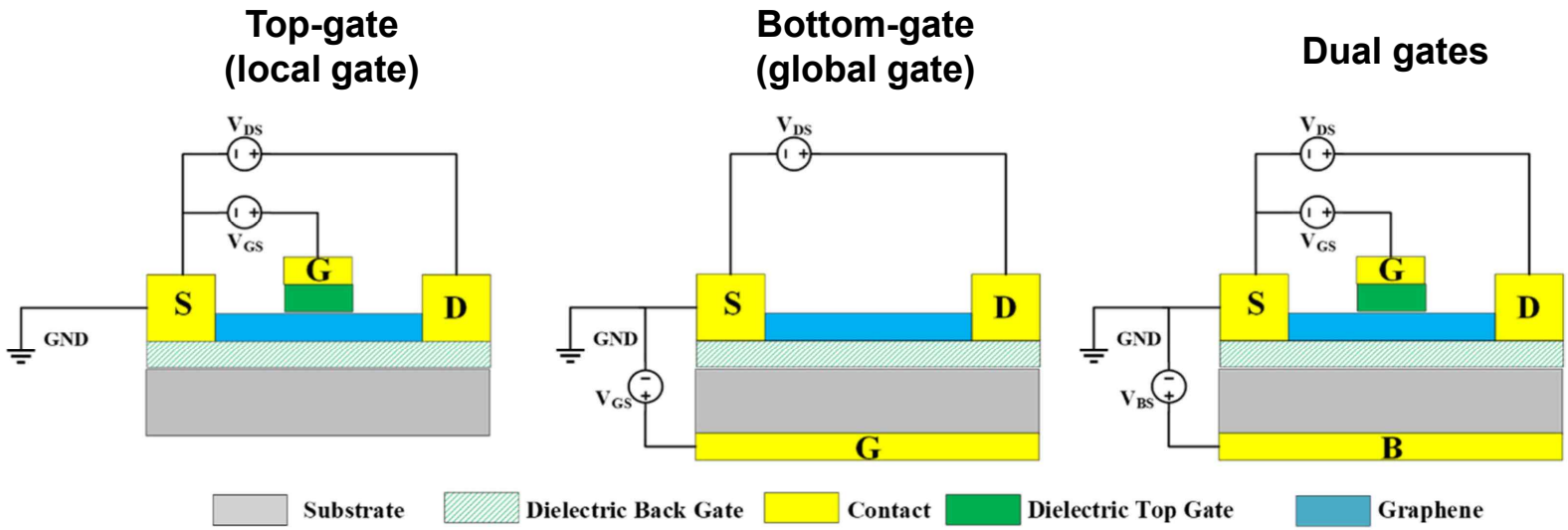

water tap

MOSFET	Tap	Common features
Electron	Water	The substance which flows
Source		Where electron(water) comes from
Drain		Where electron(water) comes out
V_{ds}	Pressure of water	Driving force, Always applied
V_g	Valve	Switching, Variable, ex) n-type FET: turn off at $V_g < 0$, turn on at $V_g > 0$

Two-probe measurement

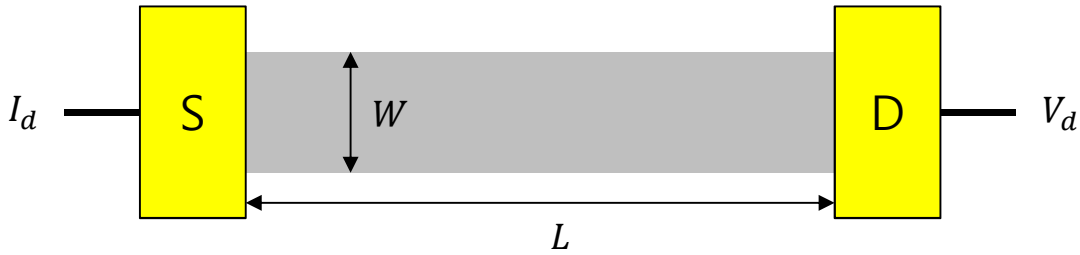

$$\rho = \frac{W}{L}\frac{V_d}{I_d}$$

$$\mu_{FE} = \frac{1}{C}\frac{d\sigma}{dV_g} = \frac{1}{C}\frac{d(1/\rho)}{dV_g} = \frac{t}{\epsilon_0\epsilon}\frac{L}{W}\left(\frac{dI_d}{dV_g}\right)\frac{1}{V_d}$$

$\epsilon_0\epsilon$: permittivity of SiO_2
t : thickness of SiO_2
I_d: drain current
V_d: source-drain voltage

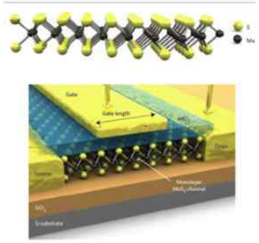

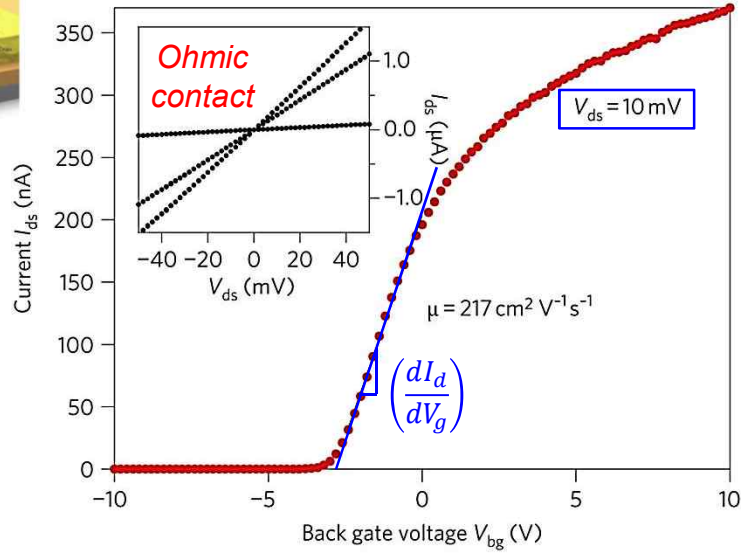

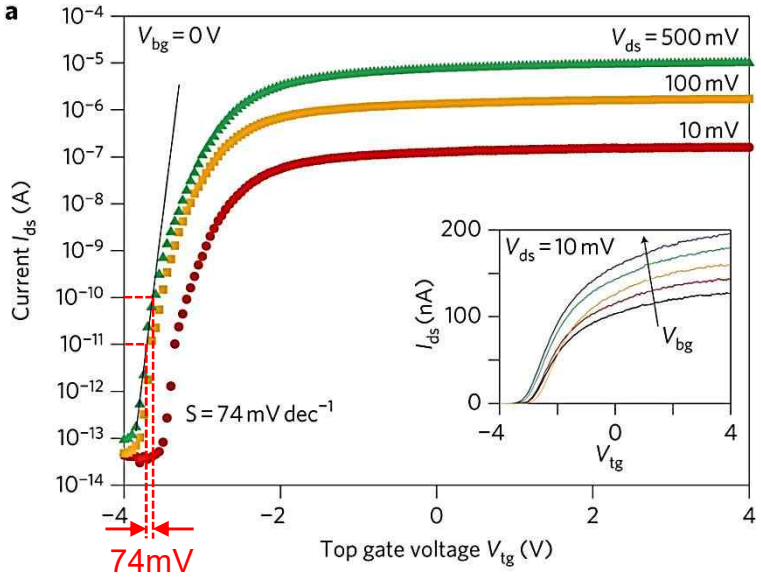

A. Kis et al. Nature Nanotechnol. (2011)

Effect of contact resistance

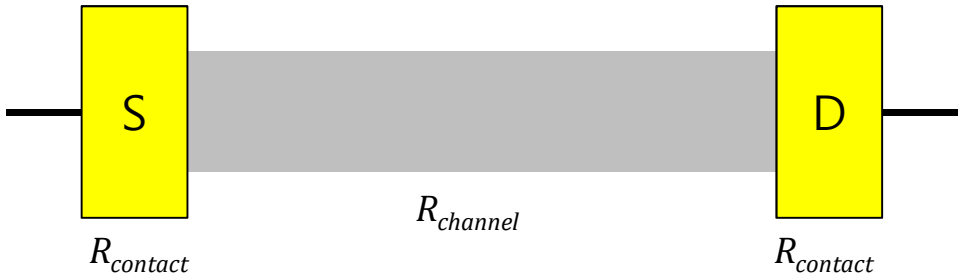

$R_{total} = V_d / I_d$

$R_{total} = 2R_{contact} + R_{channel}$

If $R_{contact} << R_{channel}$, $R_{channel} \sim V_d / I_d$

If $R_{contact} > R_{channel}$, $R_{contact} \sim V_d / I_d$ *when* $L = 0$

Because $R_{channel} = R_{sheet}\, x\, (L / W)$

Transmission Line Method / Transfer Length Method (TLM)

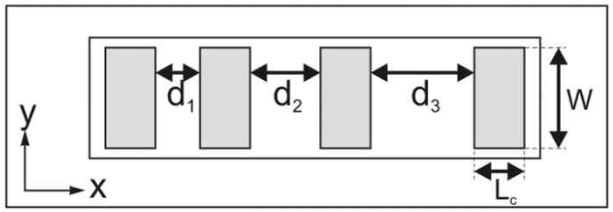

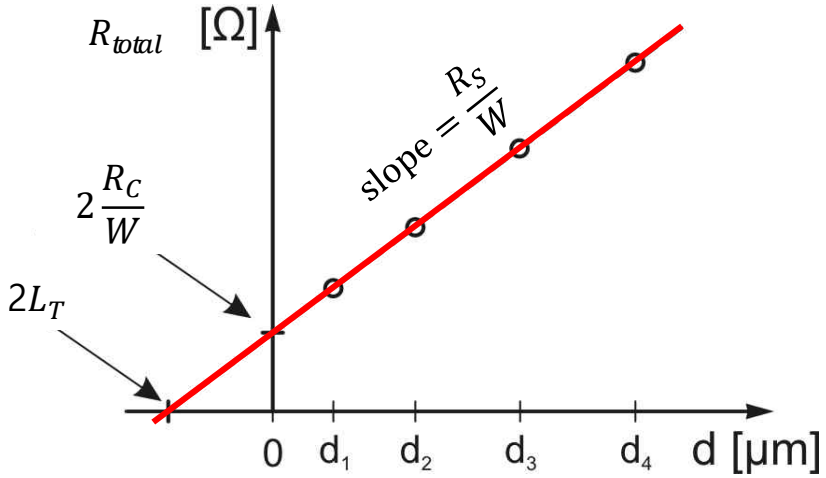

$$R_{total} = \frac{R_S}{W} d + 2\frac{R_C}{W}$$

$$L_T = \frac{R_C}{R_S}$$

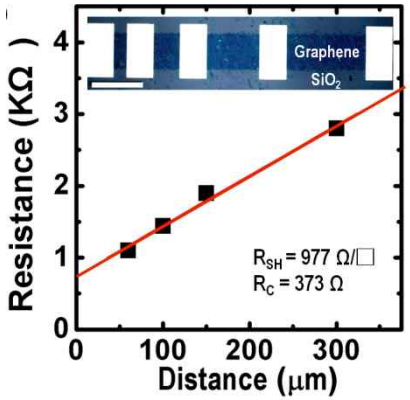

L_T : *transfer length or effective contact length*

(For validity of TLM, $L_T << L_C$*)*

TLM device of graphene

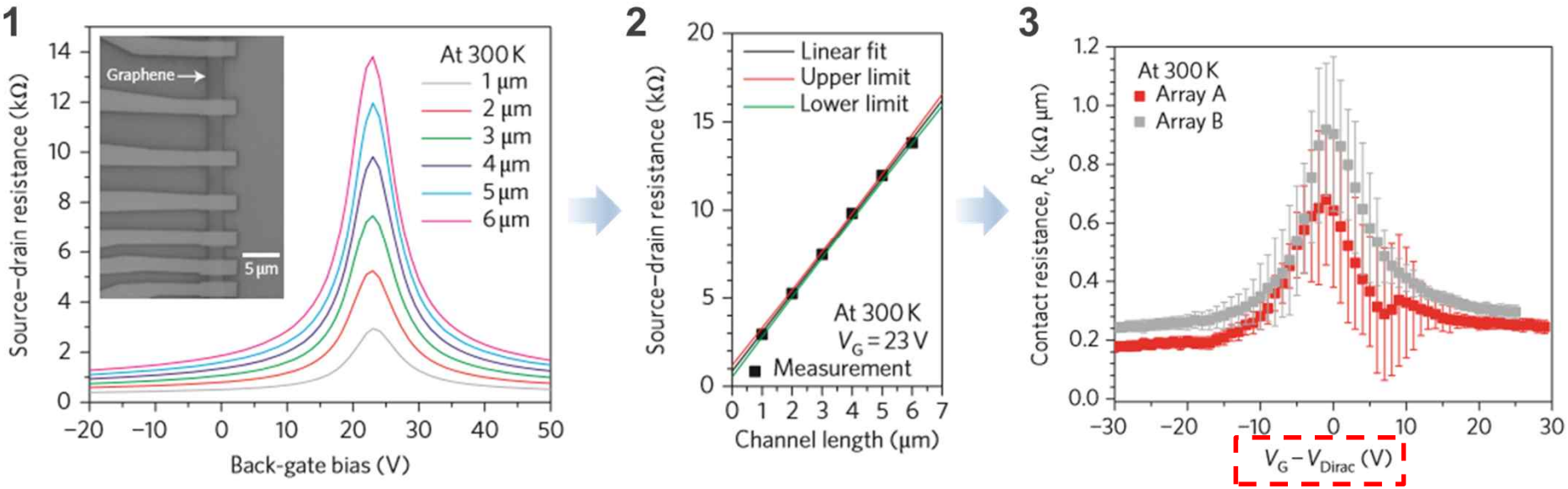

Nat. Nanotechnol. 6, 179 (2011)

$$n = \frac{\epsilon_0 \epsilon V_g}{te}$$

$n = a \times (V_G\text{-}V_{Dirac})$

For 300 nm SiO_2 ;

$a = 7.2 \times 10^{10}$ ($cm^{-2}V^{-2}$)

Improving R_C

Contacting Material	Stack layers (thickness in nm)	Deposition technique	Graphene	Measurement technique	Contact resistivity (Ωμm)	Notes
Ag	Ag		CVD	TLM	1400	*Rapid thermal annealing*
	Ag/Au (100/10)	E-Beam	Exfoliated	TLM	2000	
Au – Gold	Au		CVD	TLM	630	*Rapid thermal annealing*
	Au (20)		CVD	2p/4p	340	
	Au	E-Beam	CVD	TLM	1200	*Metal on Bottom*
	Au (20) grains	Th. Evaporator	Exfoliated	TLM	130	*Grains on whole surface*
	Au (250)	Evaporator	CVD	TLM	456	*Patterned holes in graphene/edge contact*
	Au (81)	Evaporator	CVD	TLM	500	
	Au/Cu/Au (20/200/60)	Th. Evaporator	Exfoliated	TLM	50	*Resist free fabrication process*
Co	Co/Au (100/10)	E-Beam	Exfoliated	TLM	300	
Cr – Chromium	Cr/Au (10/20)	Th. Evaporator	Exfoliated	CBK	$10^3 \div 10^6$	
	Cr/Au (100/10)	E-Beam	Exfoliated	TLM	3000	
	Cr/Au (5/150)	Sputtering	Exfoliated	2p/4p	5000	
	Cr/Pd (0.5/40)	Evaporator	Exfoliated	HTA	350 ÷ 750	
	Cr/Pd/Au (1/15/50)	E-Beam	CVD	TLM	270	*Pre-plasma treatment/ edge contact*
	Cr/Pd/Au (1/15/60)	E-Beam	Exfoliated	TLM	100	*Edge contact to encapsulated graphene in BN*
Cu – Copper	Cu		CVD	TLM	8800	
	Cu		CVD	TLM	2900	*Rapid thermal annealing*
	Cu (35)	Th. Evaporator	Exfoliated	TLM	1160	*As prepared*
	Cu (35)	Th. Evaporator	Exfoliated	TLM	620	*Annealed at 260 °C*
	Cu (50)	E-Beam	6H-SiC	2p/4p	125	*Cuts patterned*
	Cu/Au (5/50)	E-Beam	CVD	TLM	92	*Doping by PVP/PMF insulator*
Pt	Pt/Au (25/50)	Evaporator	CVD	TLM	1100	
Ti – Titanium	Ti/Al (10/70)	E-Beam	Exfoliated	2p/4p	<250	
	Ti/Au (10/20)	Th. Evaporator	Exfoliated	CBK	$10^3 \div 10^6$	
	Ti/Au (10/25)	E-Beam	Exfoliated	TLM	600 ÷ 1000	
	Ti/Au (10/40)	Evaporator	Exfoliated	2p/4p	<400	
	Ti/Au (100/10)	E-Beam	Exfoliated	TLM	800	
	Ti/Au (20/80)	E-Beam	CVD	TLM	568	*UV-ozone treatment*
	Ti/Au (5/50)	E-Beam	CVD	2p/4p	7500	
	Ti/Au (5/50)	E-Beam	CVD	TLM	23	*Doping by PVP/PMF insulator*
	Ti/Au (9/80)	E-Beam	Exfoliated	2p/4p	2000	
	Ti/Au (9/80)	Sputtering	Exfoliated	2p/4p	10^4	
	Ti/Au(70/70)	Sputtering	Exfoliated	TLM	$3 \cdot 10^4$	
	Ti/Pd/Au (0.5/20/30)	E-Beam	CVD	2p/4p	750	
	Ti/Pd/Au (0.5/30/30)	E-Beam	CVD	2p/4p	~320	*Double contact*
	Ti/Pd/Au (0.5/30/30)	E-Beam	CVD	2p/4p	~525	*Top contact*
	Ti/Pd/Au (0.5/30/30)	E-Beam	CVD	2p/4p	~715	*Bottom contact*
	Ti/Pd/Au (1.5/45/15)	E-Beam	CVD	2p/4p	200 ÷ 500	*Al cap layer*
	Ti/Pd/Au (1.5/45/15)	E-Beam	CVD	2p/4p	2000 ÷ 2500	
	Ti/Pt/Au	E-Beam	6 H-SiC	TLM	20 ÷ 80	
Fe	Fe/Au (100/10)	E-Beam	Exfoliated	TLM	2000	
Nb	Nb/Au (15/25)	Sputtering	Exfoliated	TLM	$1.9 \cdot 10^4$	
	Nb/Au (25/75)	Sputtering	Exfoliated	2p/4p	$2.4 \cdot 10^4$	
Ni – Nichel	Ni (100)	Th. Evaporator	Exfoliated	2p/4p	100	
	Ni (25)	Th. Evaporator	Exfoliated	CBK	500	
	Ni (60)	E-Beam	Exfoliated	TLM	2500	
	Ni (75)	Evaporator	CVD	TLM	2200	
	Ni/Au (100/10)	E-Beam	Exfoliated	TLM	300	
	Ni/Au (25/50)	Evaporator	CVD	TLM	400	
	Ni/Au (30/20)	E-Beam	CVD	2p/4p	2100	
	Ni/Au(70/50)	Sputtering	Exfoliated	TLM	7000	
	Ni/Cu/Au (20/200/60)	Th. Evaporator	Exfoliated	2p/4p	1000	
Pd – Palladium	Pd		CVD	TLM	570	*Rapid thermal annealing*
	Pd (50)	E-Beam	6H-SiC	2p/4p	457	*Cuts patterned*
	Pd (75)	Evaporator	CVD	TLM	970	
	Pd/Au (100/10)	E-Beam	Exfoliated	TLM	600	
	Pd/Au (20/30)	Th. Evaporator	CVD	2p/4p	200 ÷ 400	*Antidote arrays under metal electrode*
	Pd/Au (20/60)	E-Beam	CVD	2p/4p	88	*Laser cleaning of contact area*
	Pd/Au (25/25)		Exfoliated	TLM	230 ÷ 900	*Bias dependent*
	Pd/Au (30/50)	E-Beam	Exfoliated	TLM	69	
	Pd/Au (5/50)	E-Beam	CVD	TLM	122	*Doping by PVP/PMF insulator*

Prog. Surf. Sci. 92, 143-175 (2017)

Is Graphene Contacting with Metal Still Graphene?

K. Nagashio*, T. Moriyama, R. Ifuku, T. Yamashita, T. Nishimura and A. Toriumi
Department of Materials Engineering, The University of Tokyo
7-3-1, Hongo, Bunkyo-ku, Tokyo 113-8656, Japan
*nagashio@material.t.u-tokyo.ac.jp

Abstract:

This paper focuses both electrical transport and Raman characteristics of graphene underneath the metal. We have found that there is only a weak interaction between metal and graphene, while graphene is significantly affected by the substrate underneath graphene.

to the Fermi level to induce carriers. The most striking consequence in this work is that Ni does not affect graphene characteristics, which means that the band structure alternation by defect formation and π-d coupling is negligibly small. The linear dispersion in graphene is obviously maintained. Main thing that takes place at the metal/graphene interface is the charge transfer, although the degree of the band alternation by the graphene/metal interaction should be studied quantitatively.

On the other hand, the band calculation [8] and experimental characterization of graphene grown on Ni(111) [9] suggest that the linear dispersion is strongly altered by the π-d coupling for graphene contacting transition metals.

shift, which implies that the bonding interaction at metal/graphene is unexpectedly weak, and (ii) the doping type in graphene is affected by "mixed" interactions with metal and substrate. These findings are crucial to control FET properties.

In search of quantum-limited contact resistance: understanding the intrinsic and extrinsic effects on the graphene–metal interface

Anindya Nath[1,2], Marc Currie[2], Anthony K Boyd[2], Virginia D Wheeler[2], Andrew D Koehler[2], Marko J Tadjer[2], Zachary R Robinson[3], Karthik Sridhara[4], Sandra C Hernandez[2], James A Wollmershauser[2], Jeremy T Robinson[2], Rachael L Myers-Ward[2], Mulpuri V Rao[1] and D Kurt Gaskill[2]

[1] George Mason University, 4400 University Dr Fairfax, Virginia, VA 22030, USA
[2] US Naval Research Laboratory, 4555 Overlook Ave., SW, Washington, DC 20375, USA
[3] The College at Brockport, SUNY, 350 New Campus Dr, Brockport, NY 14420, USA
[4] Texas A&M University, 401 Joe Routt Blvd, College Station, TX 77843, USA

probability, as exemplified by the Landauer–Büttiker model, which is dependent on the presence or absence of end-contacts and dopant/work-function mediated conduction. The model predicts the need for both end-contacts and a clean graphene–metal interface as necessary conditions to approach quantum limited contact resistance.

2D Mater. 3 025013 (2016)

Doping Graphene with Metal Contacts

G. Giovannetti,[1,2] P. A. Khomyakov,[2] G. Brocks,[2] V. M. Karpan,[2] J. van den Brink,[1,3] and P. J. Kelly[2]

[1]*Instituut-Lorentz for Theoretical Physics, Universiteit Leiden, P.O. Box 9506, 2300 RA Leiden, The Netherlands*
[2]*Faculty of Science and Technology and MESA+ Institute for Nanotechnology, University of Twente, P.O. Box 217, 7500 AE Enschede, The Netherlands*
[3]*Institute for Molecules and Materials, Radboud Universiteit, Nijmegen, The Netherlands*

(Received 15 February 2008; published 10 July 2008)

Making devices with graphene necessarily involves making contacts with metals. We use density functional theory to study how graphene is doped by adsorption on metal substrates and find that weak bonding on Al, Ag, Cu, Au, and Pt, while preserving its unique electronic structure, can still shift the Fermi level with respect to the conical point by ~0.5 eV. At equilibrium separations, the crossover from p-type to n-type doping occurs for a metal work function of ~5.4 eV, a value much larger than the graphene work function of 4.5 eV. The numerical results for the Fermi level shift in graphene are described

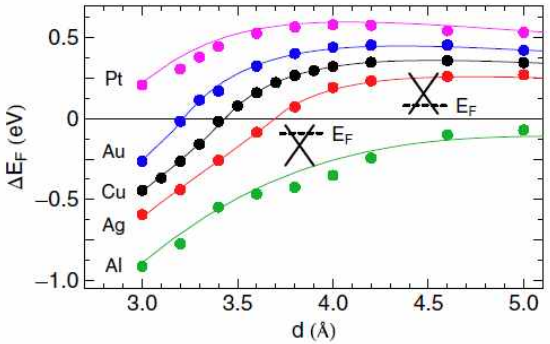

FIG. 5 (color online). Fermi level shifts $\Delta E_F(d)$ as a function of the graphene-metal surface distance. The dots give the calculated DFT results, the solid lines give the results obtained from the model, Eq. (1) [23].

PRL 101, 026803 (2008)

Formation of “Good” Contacts

Metal types

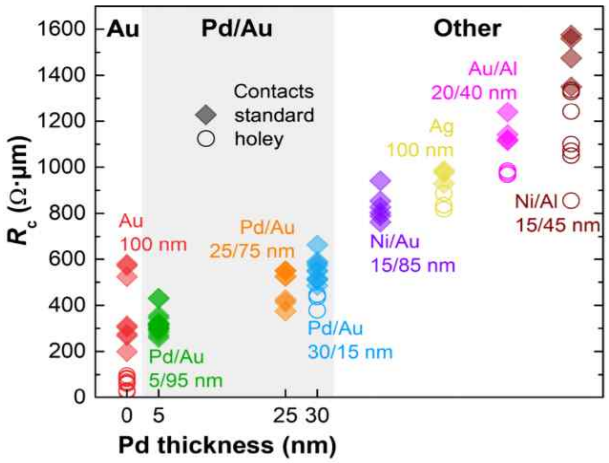

2D Mater. 5, 025014 (2018)

Edge contacts

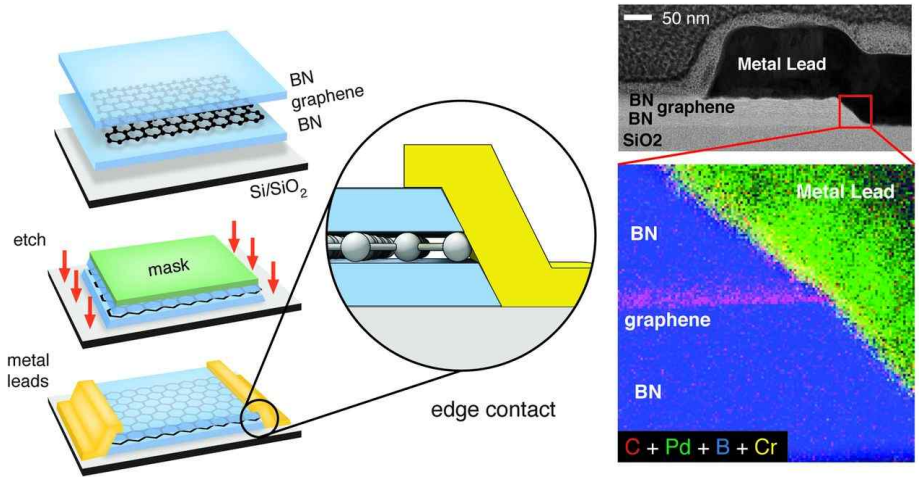

Science 342, 614 (2013)

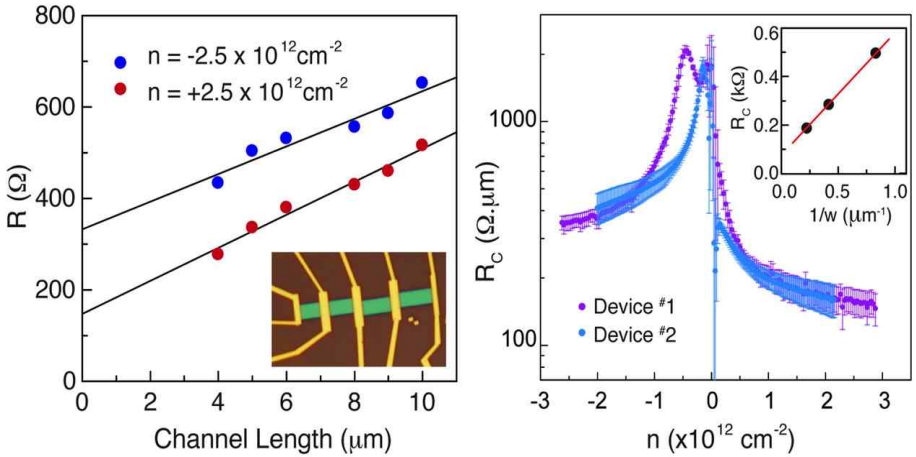

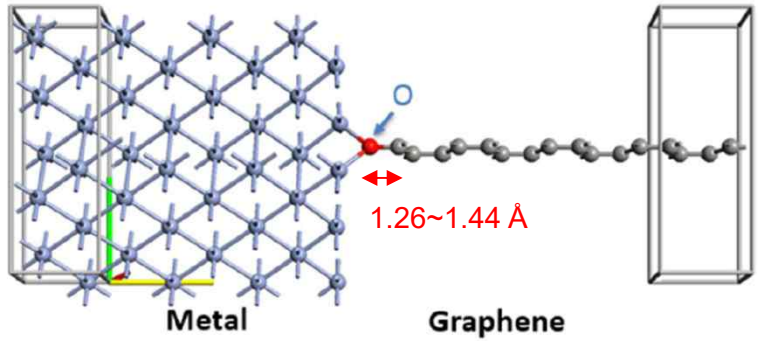

- Short distance of metal and interfacial atom (O) induces overlapped orbitals, which promote transport of charges at contacts

Formation of “Good” Contacts

Combination of edge & top contacts

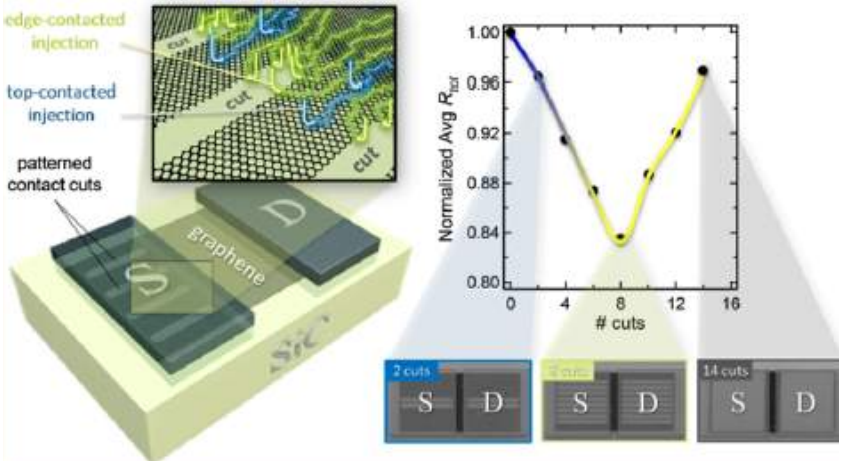

Acs Nano 7, 3661–3667 (2013)

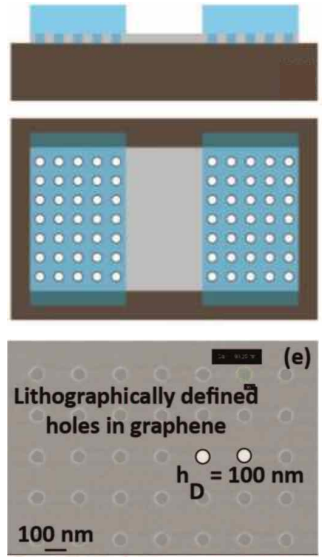

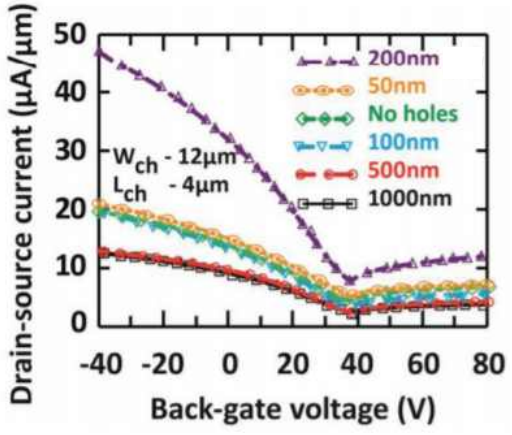

Adv. Mater. Interfaces 1801285 (2018)

Laser nano-welding

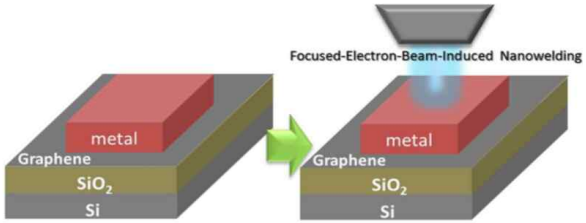

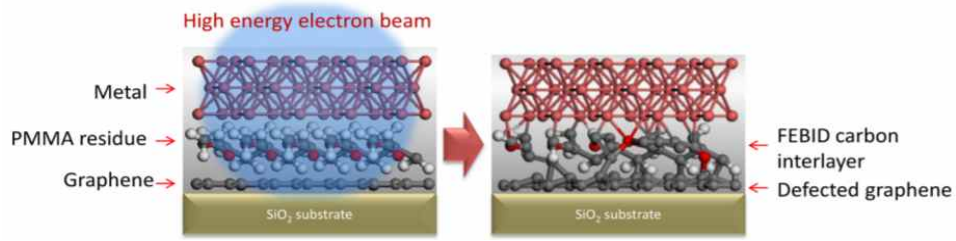

ACS Nano 10, 1, 1042-1049 (2016)

Fluorinated Graphene Contacts

Graphene etch mask and etch stop

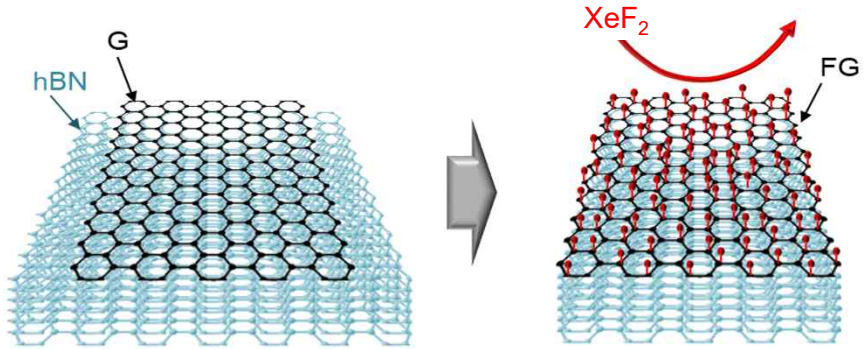

- Selective etching with atomic precision
- Atomic scale etch masks and etch stops

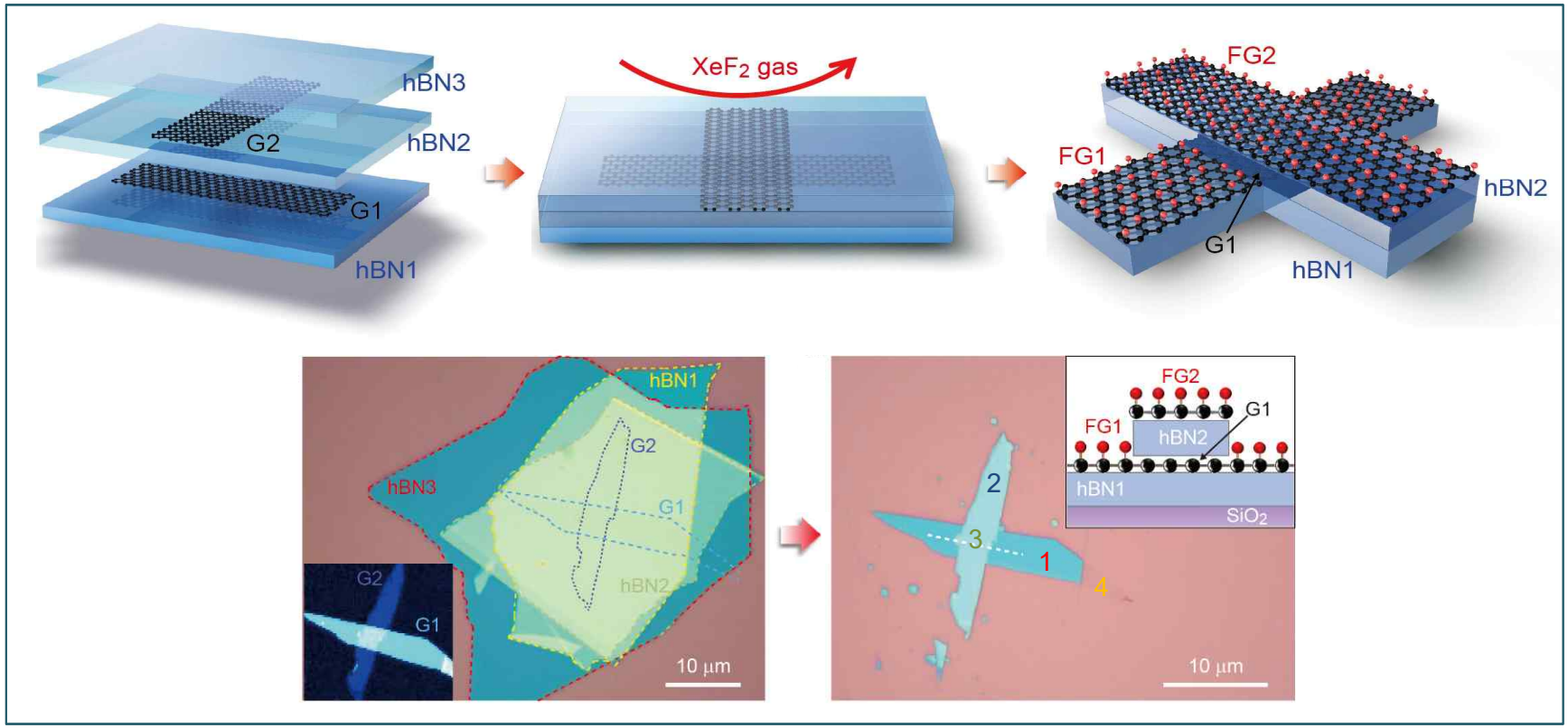

J.Y. Son, J.Y. Kwon, G.H. Lee, A. van der Zande* **Nature Communications** 9, 3988 (2018)*

Fluorinated Graphene Contacts

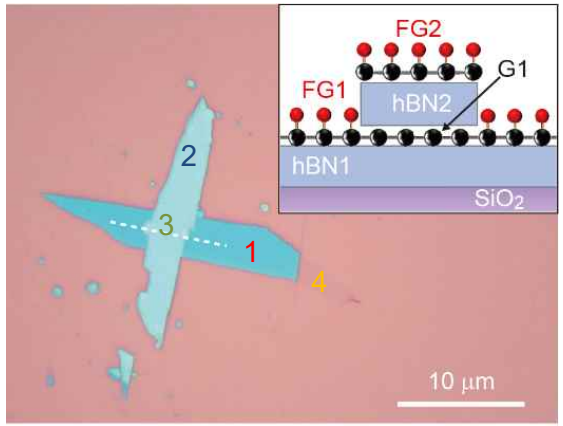

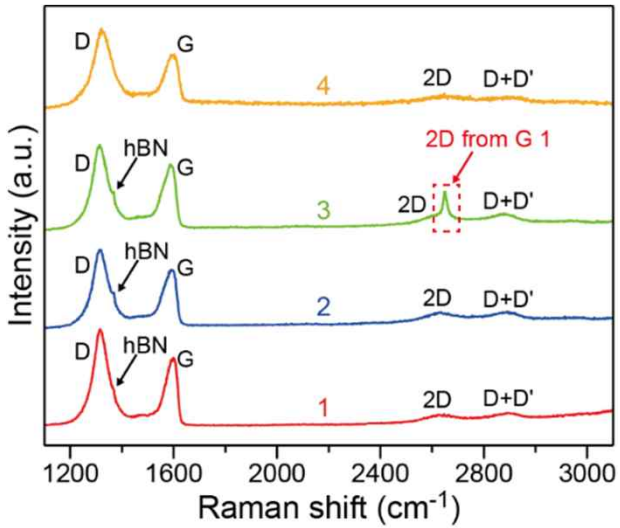

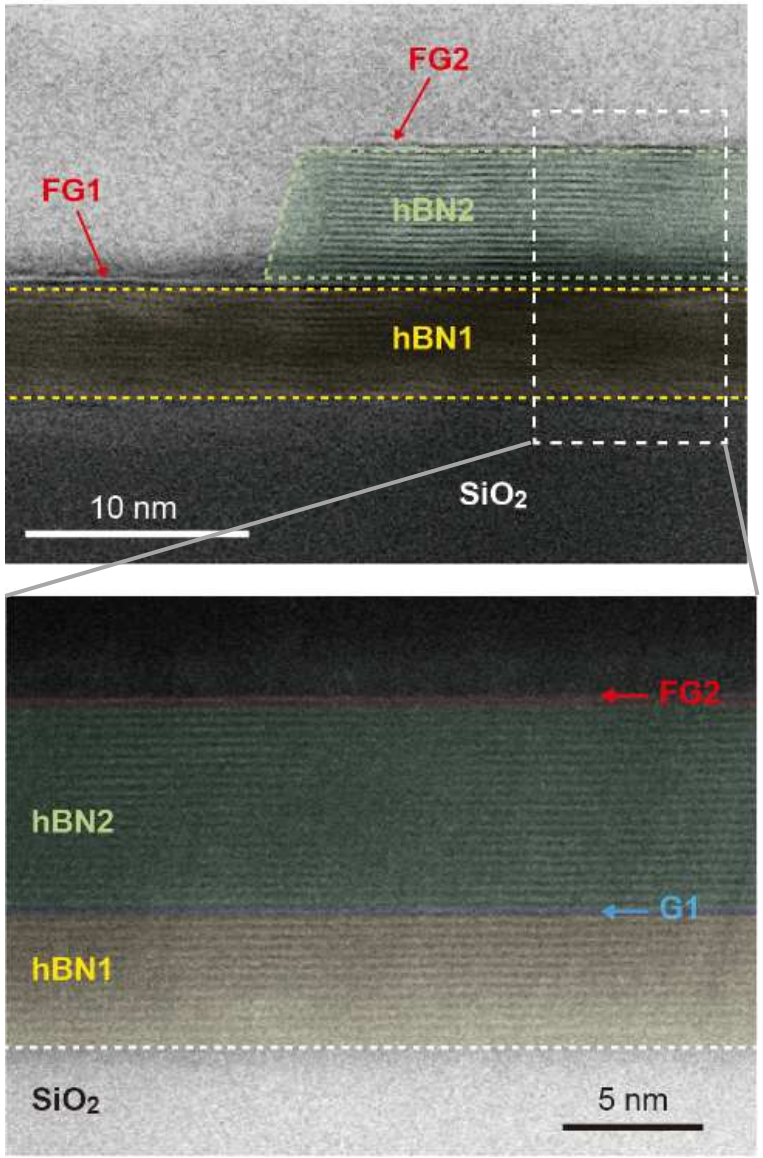

- Graphene can be used as etch masks and etch stops.
- hBN under graphene remains unchanged.
- FG is impermeable to gases.

J.Y. Son, J.Y. Kwon, G.H. Lee, A. van der Zande** ***Nature Communications*** *9, 3988 (2018)*

Fluorinated Graphene Contacts

Fabrication process

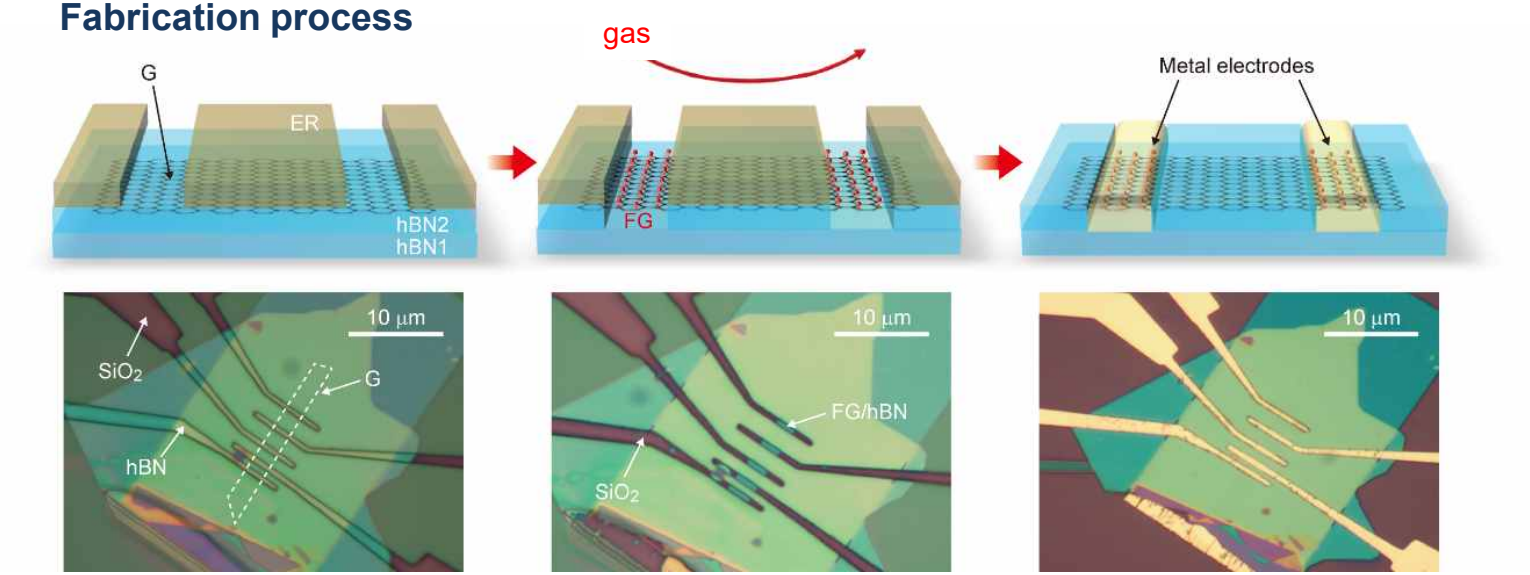

hBN-encapsulated GEFT with via contacts

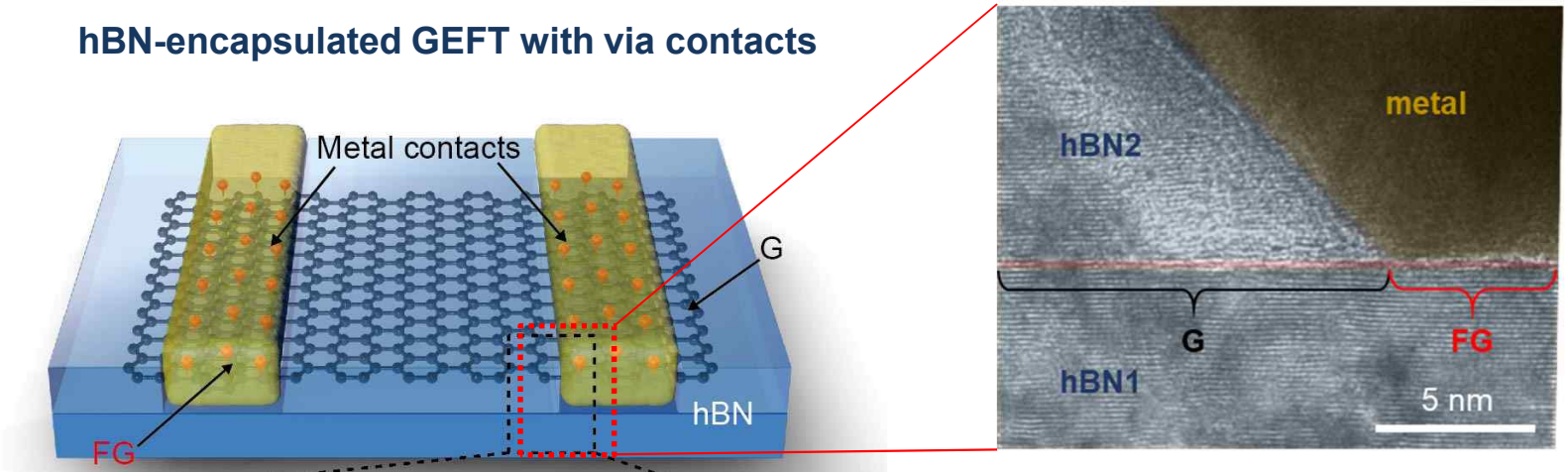

J.Y. Son, J.Y. Kwon, G.H. Lee, A. van der Zande* **Nature Communications** 9, 3988 (2018)*

Fluorinated Graphene Contacts

TLM method

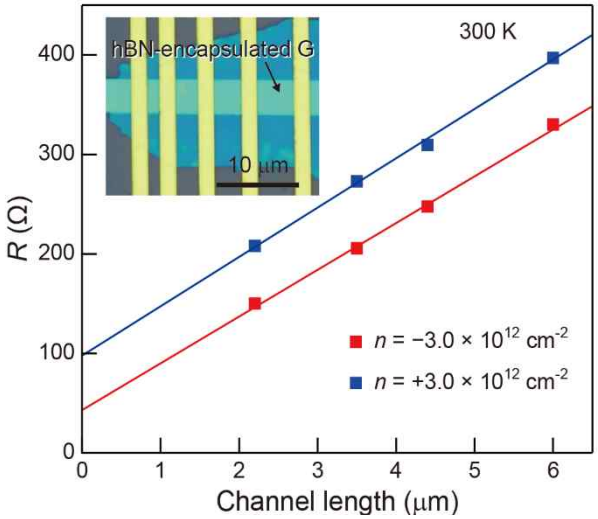

Reliability at low T

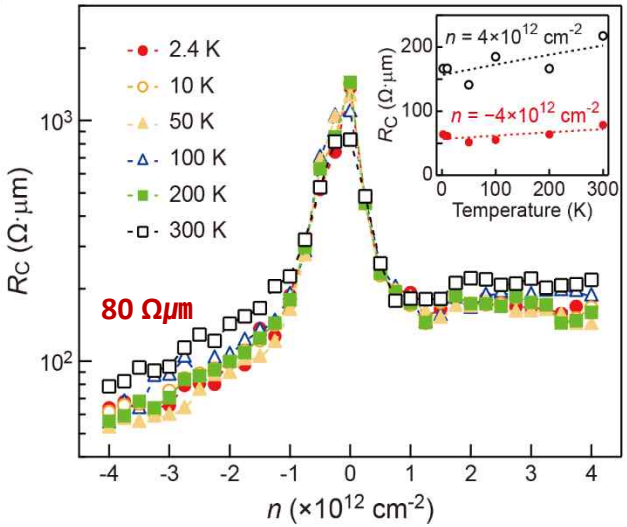

Carrier mobility

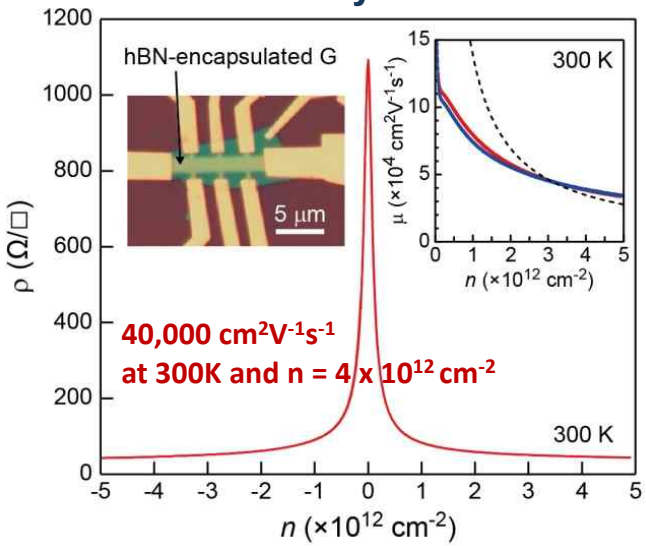

Low-T measurement

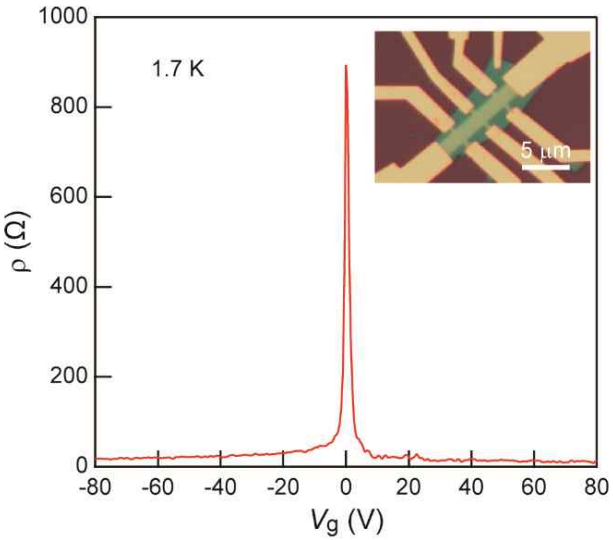

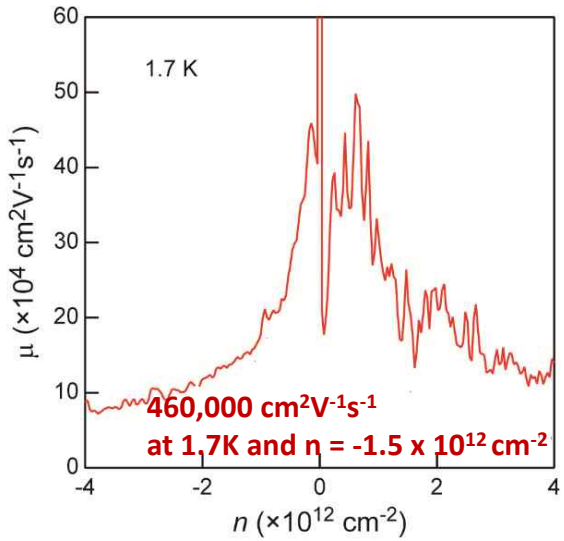

- One-step process for formation of via contacts
- High performance of graphene device with via contacts
- R_c ~ 80 Ωμm and μ = 40,000 cm^2/Vs at RT
- High stability and reliability of via contacts

J.Y. Son, J.Y. Kwon, G.H. Lee, A. van der Zande** **Nature Communications** *9, 3988 (2018)*

Fluorinated Graphene Contacts

Simulation of charge transfer at interface of metal and graphene

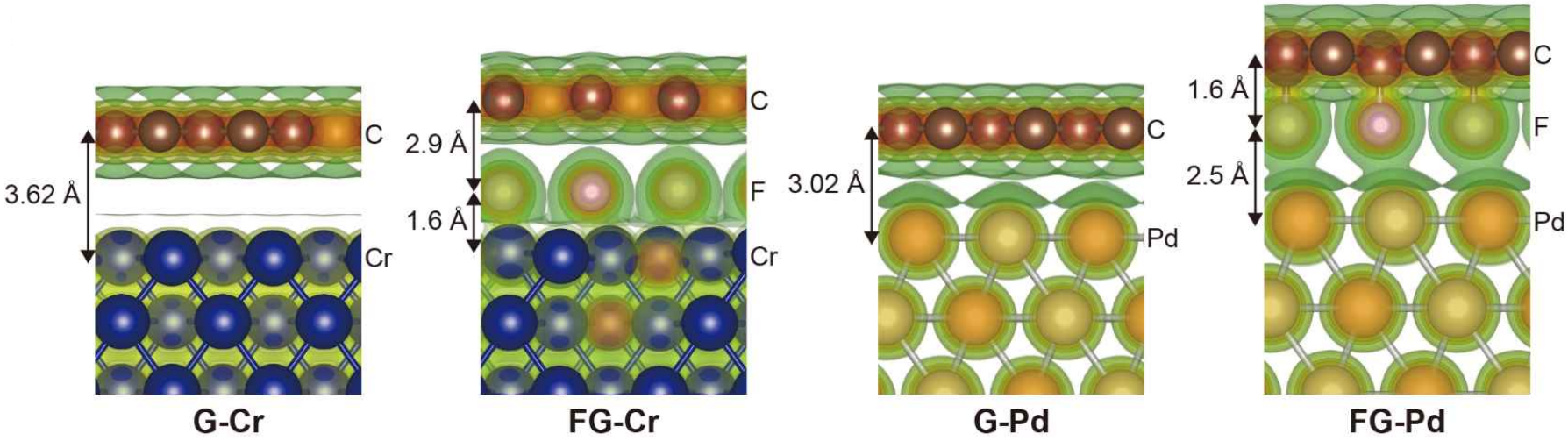

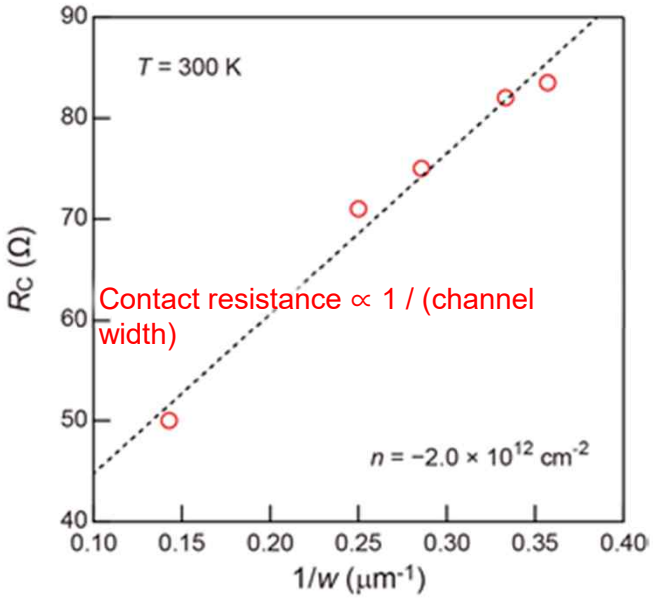

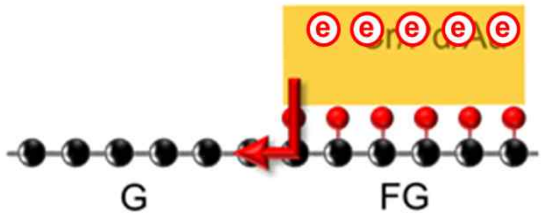

- Charge transfer is more efficient in FG via contacts due to smaller spacing of C-F-Cr and C-F-Pd.
- Contact resistance is reversely proportional to channel width of graphene.
- Charge injection of FG via contact is dominant at the edge of graphene-FG interface.

J.Y. Son, J.Y. Kwon, G.H. Lee, A. van der Zande** ***Nature Communications*** *9, 3988 (2018)*

3D-integrated Graphene Devices

One-step fabrication process

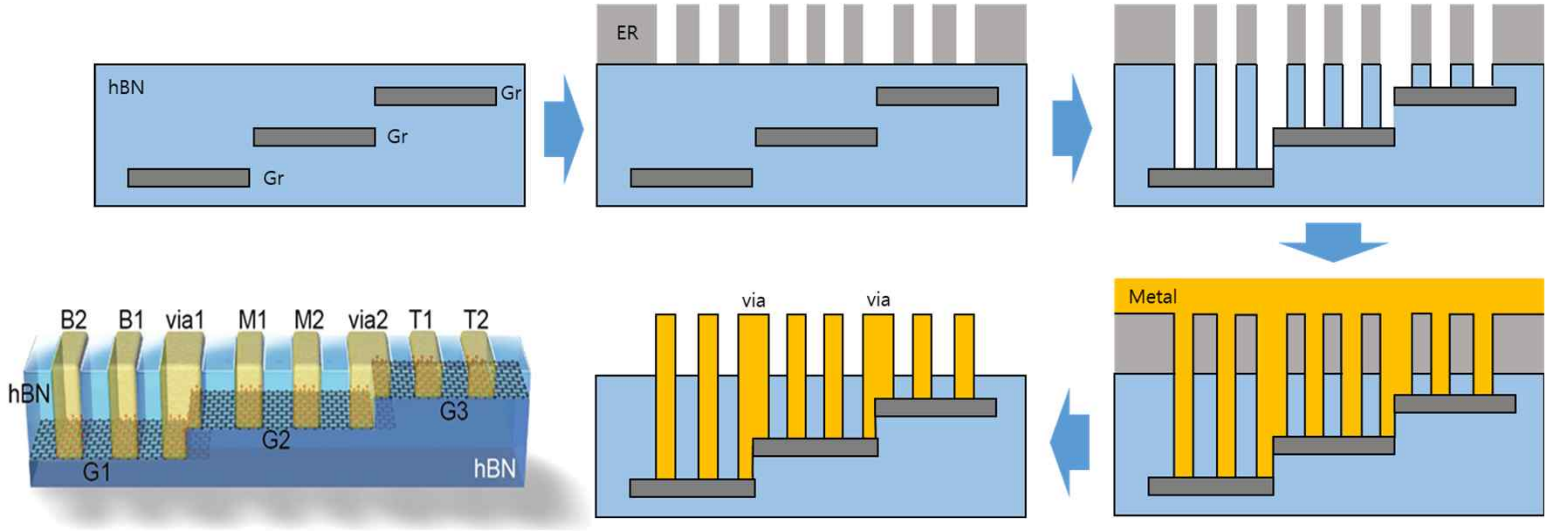

Multi-stacked GFETs

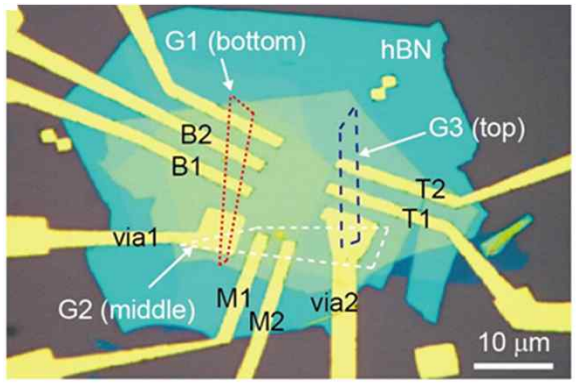

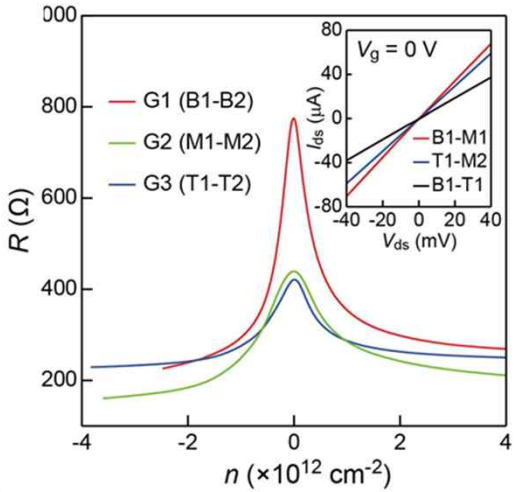

J.Y. Son, J.Y. Kwon, G.H. Lee, A. van der Zande** **Nature Communications** *9, 3988 (2018)*

Graphene Via Contact Architecture

Graphene via contact architecture

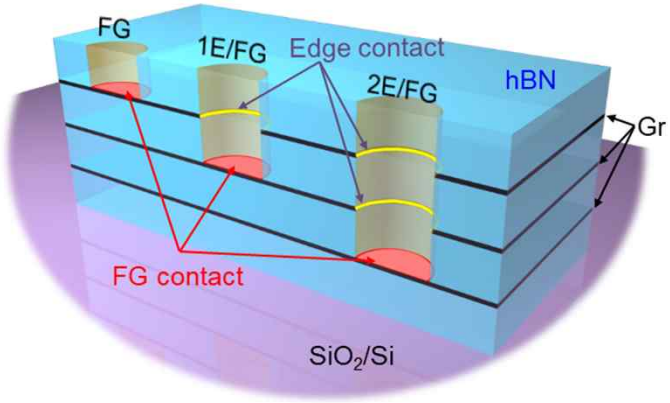

Step-by-step fabrication process of via contact

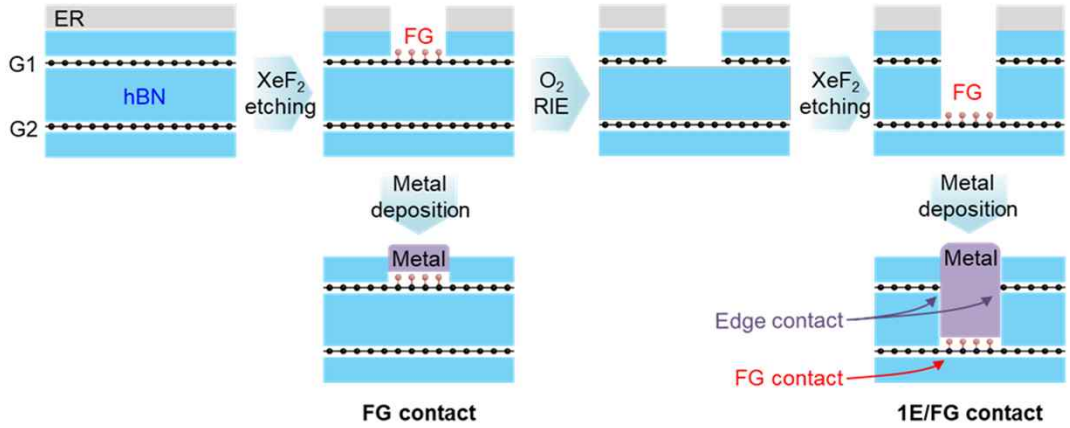

Electrical measurements and TEM analysis

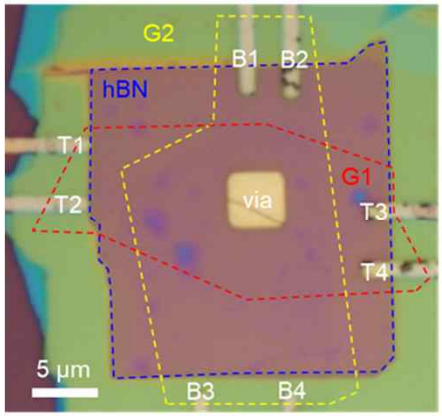

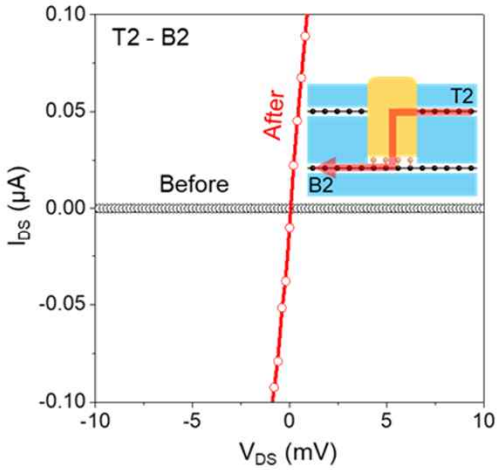

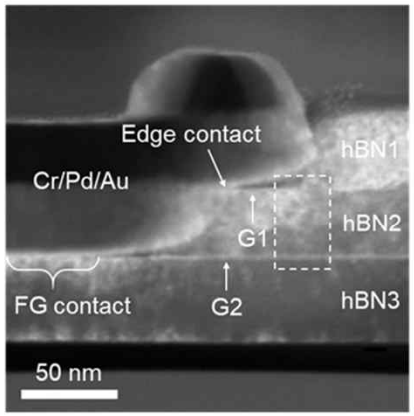

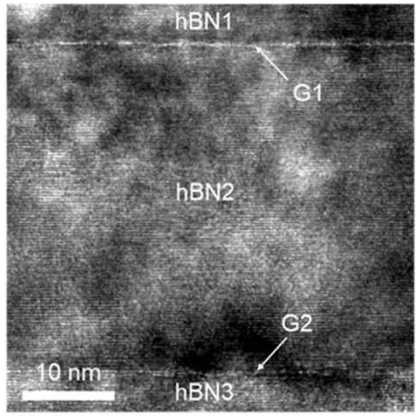

Y. Shin, J.Y. Kwon, G.H. Lee* **Small** (2022)

Graphene Via Contact Architecture

hBN-encapsulated TMD-FET with via contacts

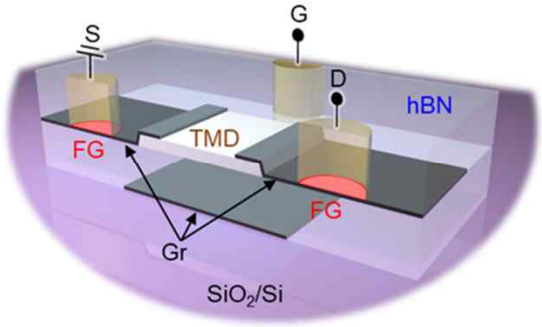

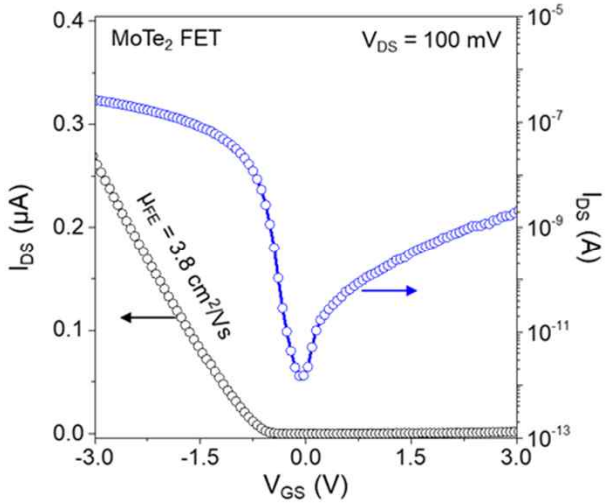

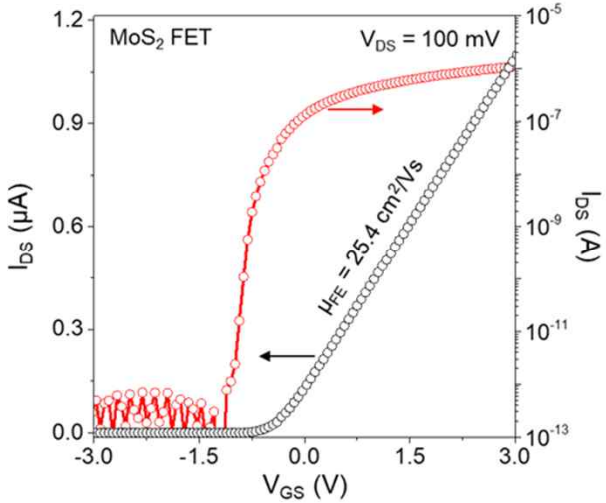

Vertically integrated CMOS inverter with FG, 1E/FG via contacts

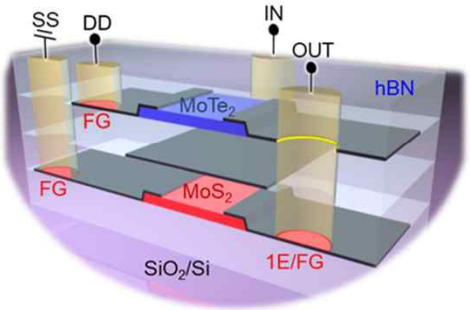

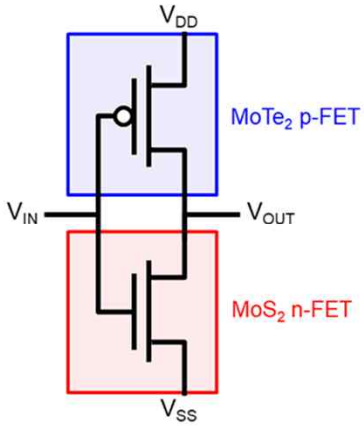

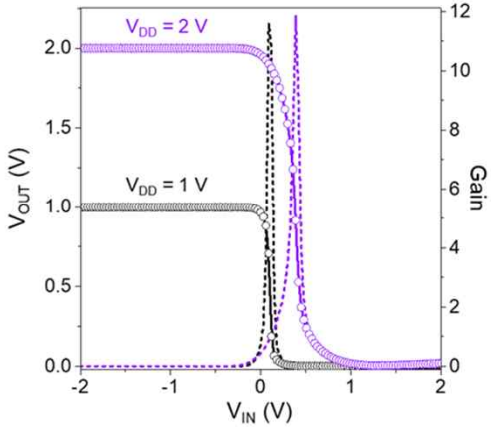

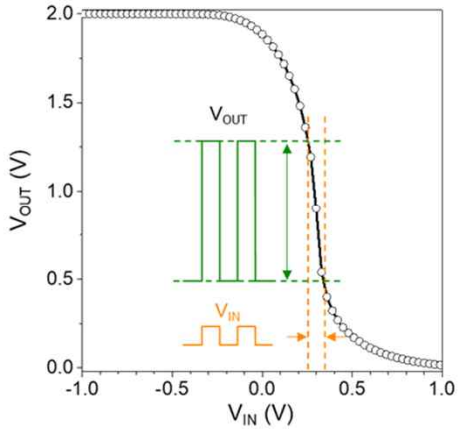

Y. Shin, J.Y. Kwon, G.H. Lee* **Small** (2022)

Carrier mobility

: How quickly an electron or hole can move through a metal or semiconductor, when pulled by an electric field.

Drift velocity in an electric field

$$v_d = \mu E$$

E : magnitude of the electric field applied to a material
v_d : magnitude of the electron drift velocity caused by the electric field
μ : electron mobility

Conductivity

$$\sigma = ne\mu = e(n\mu_e + p\mu_h).$$

n & p : number densities of electrons and holes
μ_e & μ_h : mobilities of electron and hole

Boltzmann transport equation

$$\frac{df}{dt} = \frac{\mathbf{F_t}}{\hbar} \cdot \nabla_{\mathbf{k}} f(\mathrm{k}) + \mathrm{v} \cdot \nabla_{\mathbf{r}} f(\mathrm{k}) + \frac{\partial \mathrm{f}}{\partial \mathrm{t}}$$

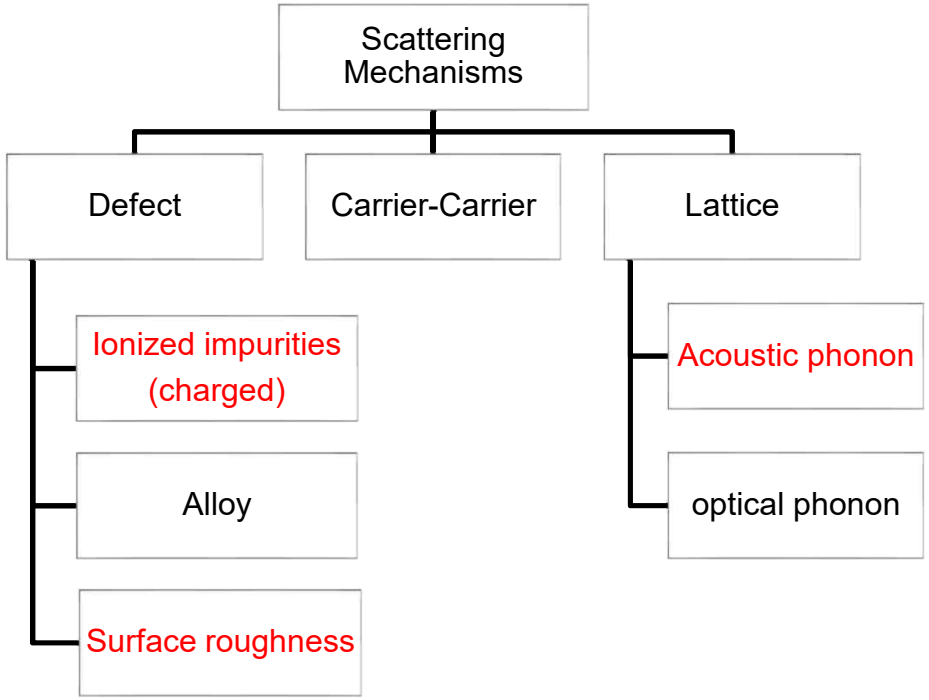

Scattering Mechanism in Graphene

(1) Short-range scattering
: Lattice defect ~ constant

(2) Long-range scattering
: Scattering form ripple, charged impurity
(depending on carrier density)

At small V_g
short range scattering dominates.
slope of linear curve proportional to carrier mobility
(high k → reduced short range scattering)

At high V_g
long range scattering dominates.
constant conductivity (as n increases, μ decreases.)
(high k → increased long range scattering)

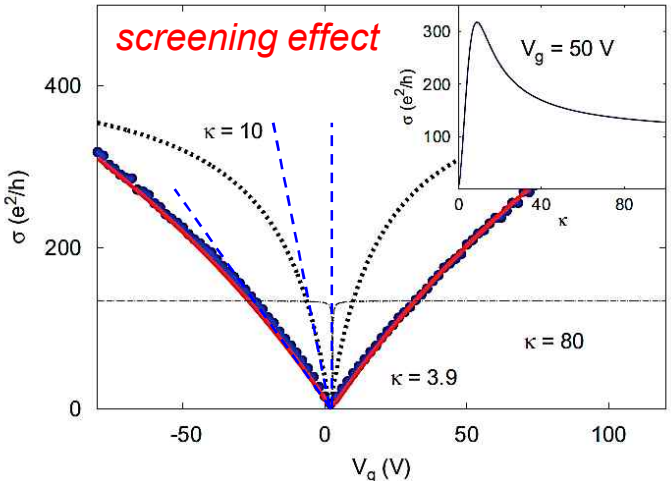

Fig. 1. This shows the dependence of conductivity on substrate dielectric constant κ. Filled blue circles show experimental data of Ref. [2]. Solid, dashed and broken lines show theoretical results for $\kappa = 3.9, 10, 80$, respectively. For large κ short-range scattering dominates while for small κ Coulomb scattering dominates. The inset shows that for a fixed gate voltage, the conductivity has a non-monotonic dependence on κ which is a consequence of the competition between short-range and long-range scattering.

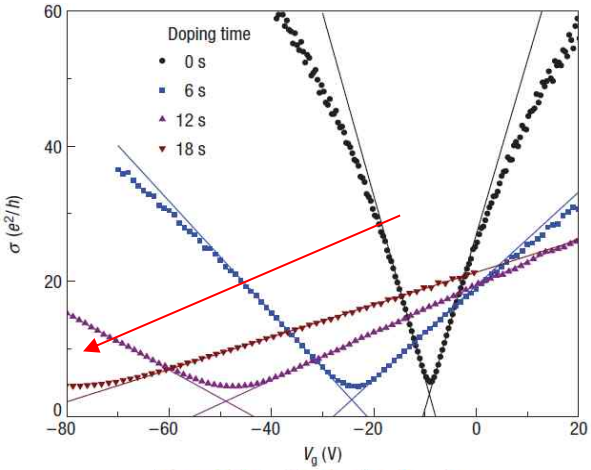

Figure 2 Potassium doping of graphene.

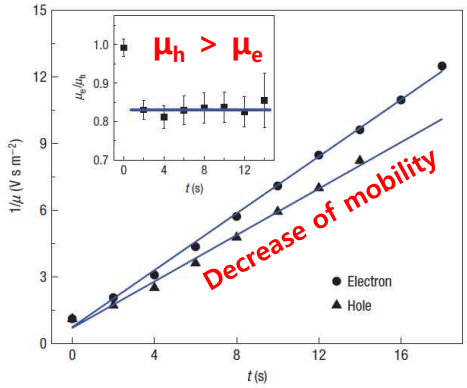

Effect of doping on μ_e is bigger than that on μ_h

By doping (substitution of impurities)

long-range scattering is more dominant.
Increased doping reduces mobility.
(smaller slope)

S. Adam et al. Physica E (2008); J. -H. Chen et al. New J. Phys. (2008)

Transport and scattering mechanism for 2D materials

- Acoustic & optical phonon scattering
- Coulomb scattering (ionized impurities)
- Surface interface phonon scattering
- Roughness scattering

Matthiessen's rule

$$\mu_0(n,T)^{-1} = \mu_{\mathrm{ph}}(T)^{-1} + \mu_{\mathrm{CI}}(n,T)^{-1} + \mu_{\mathrm{sr}}^{-1}$$

$$\frac{1}{\mu} = \frac{1}{\mu_{\mathrm{impurities}}} + \frac{1}{\mu_{\mathrm{lattice}}} + \frac{1}{\mu_{\mathrm{defects}}} + \cdots$$

$$\frac{1}{\tau} = \frac{1}{\tau_{\mathrm{impurities}}} + \frac{1}{\tau_{\mathrm{lattice}}} + \frac{1}{\tau_{\mathrm{defects}}} + \cdots$$

Temperature dependency of carrier mobility in 2D materials

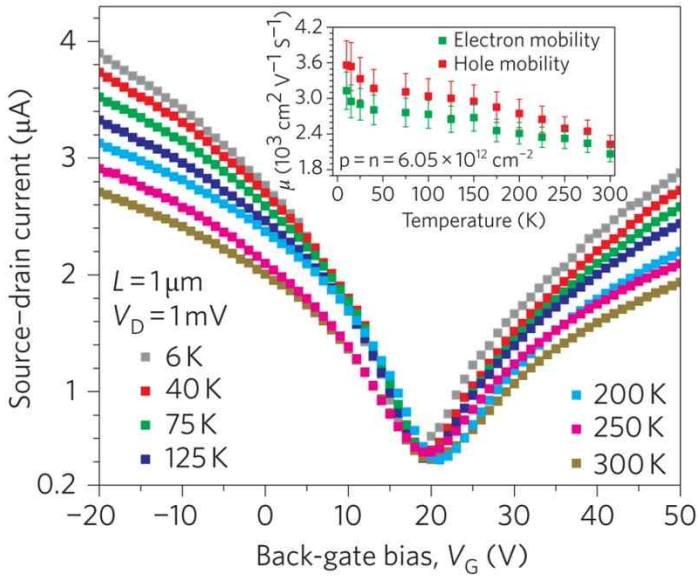

F. Xia et al. Nature Nanotechnol. (2011)

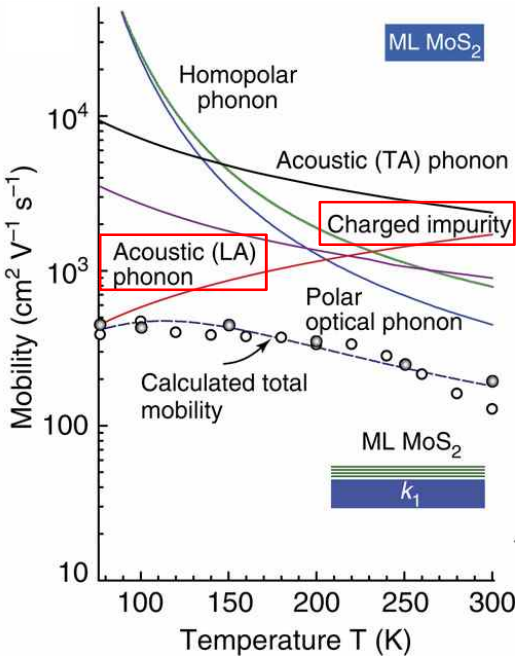

S. Kim et al. Nature Commun. (2012)

- The temperature dependencies of these scattering mechanism can be determined by $\mu \sim T^{-\gamma}$.
- At lower temperatures, ionized impurity scattering dominates, while at higher temperatures, phonon scattering dominates.

Temperature dependence of mobility			
	Si	Ge	GaAs
Electrons	$\propto T^{-2.4}$	$\propto T^{-1.7}$	$\propto T^{-1.0}$
Holes	$\propto T^{-2.2}$	$\propto T^{-2.3}$	$\propto T^{-2.1}$

Doping issue in 2D Materials

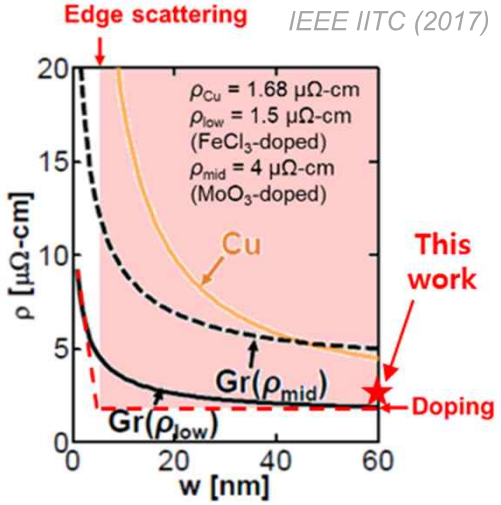

IEEE IITC (2017)

For highly conductive graphene, doping is required. However, doping induces degradation in mobility.

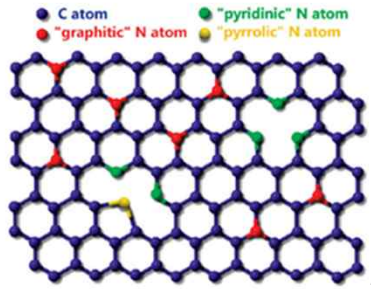

Nano Letters (2009)

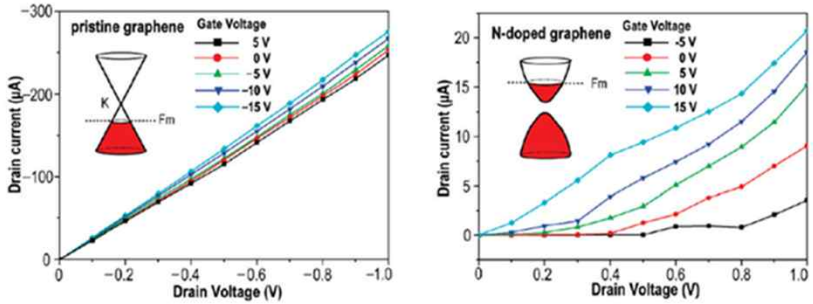

Doping of graphene by charge transfer

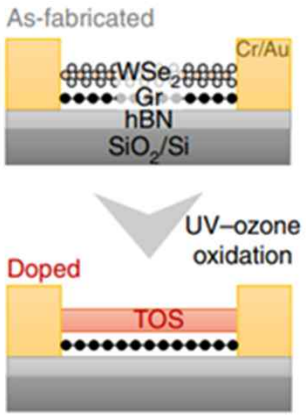

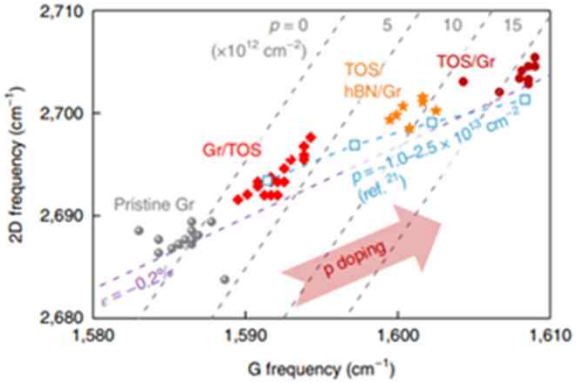

Nature Electronics (2021)

Remote doping of TMDs

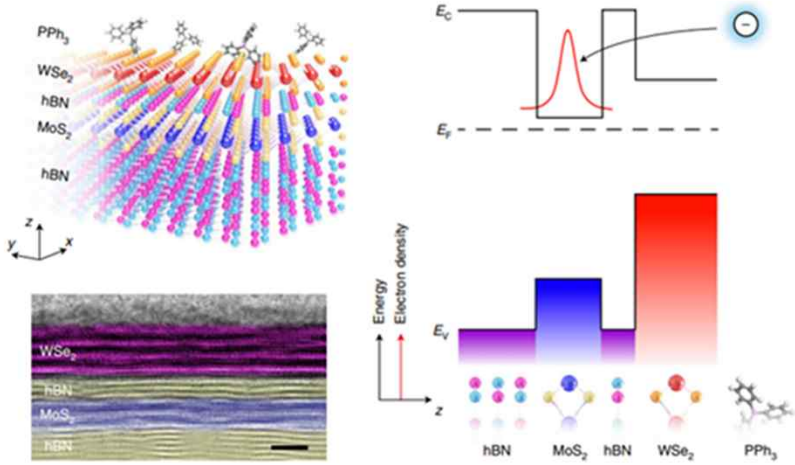

Nature Electronics (2021)

Transparency of Graphene

Fine Structure Constant Defines Visual Transparency of Graphene

R. R. Nair,[1] P. Blake,[1] A. N. Grigorenko,[1] K. S. Novoselov,[1] T. J. Booth,[1] T. Stauber,[2] N. M. R. Peres,[2] A. K. Geim[1]*

There are few phenomena in condensed matter physics that are defined only by the fundamental constants and do not depend on material parameters. Examples are the resistivity quantum, h/e^2, that appears in a variety of transport experiments, including the quantum Hall effect and universal conductance fluctuations, and the magnetic flux quantum, $h/2e$, playing an important role in the physics of superconductivity (h is Planck's constant and e the electron charge). By and large, it requires sophisticated facilities and special measurement conditions to observe any of these phenomena. In contrast, we show that the opacity of suspended graphene (*1*) is defined solely by the fine structure constant, $\alpha = e^2/\hbar c \approx 1/137$ (where c is the speed of light), the parameter that describes coupling between light and relativistic electrons and that is traditionally associated with quantum electrodynamics rather than materials science. Despite being only one atom thick, graphene is found to absorb a significant ($\pi\alpha = 2.3\%$) fraction of incident white light, a consequence of graphene's unique electronic structure.

It was recently argued (*2*, *3*) that the high-frequency (dynamic) conductivity G for Dirac fermions (*1*) in graphene should be a universal constant equal to $e^2/4\hbar$ and different from its universal dc conductivity, $4e^2/\pi h$ [however, the experiments do not comply with the prediction for dc conductivity (*1*)]. The universal G implies (*4*) that observable quantities such as graphene's optical transmittance T and reflectance R are also universal and given by $T \equiv (1 + 2\pi G/c)^{-2} = (1 + \frac{1}{2}\pi\alpha)^{-2}$ and $R \equiv \frac{1}{4}\pi^2\alpha^2 T$ for the normal light incidence. In particular, this yields graphene's opacity $(1 - T) \approx \pi\alpha$ [this expression can also be derived by calculating the absorption of light by two-dimensional Dirac fermions with Fermi's golden rule (*5*)]. The origin of the optical properties being defined by the fundamental constants lies in the two-dimensional nature and gapless electronic spectrum of graphene and does not directly involve the chirality of its charge carriers (*5*).

We have studied specially prepared graphene crystals (*5*) such that they covered submillimeter apertures in a metal scaffold (Fig. 1A inset). Such large one-atom-thick membranes suitable for optical studies were previously inaccessible (*6*). Figure 1A shows an image of one of our samples in transmitted white light. In this case, we have chosen to show an aperture that is only partially covered by suspended graphene so that opacities of different areas can be compared. The line scan across the image qualitatively illustrates changes in the observed light intensity. Further measurements (*5*) yield graphene's opacity of $2.3 \pm 0.1\%$ and negligible reflectance (<0.1%), whereas optical spectroscopy shows that the opacity is practically independent of wavelength, λ (Fig. 1B) (*5*). The opacity is found to increase with membranes' thickness so that each graphene layer adds another 2.3% (Fig. 1B inset). Our measurements also yield a universal dynamic conductivity $G = (1.01 \pm 0.04)$ $e^2/4\hbar$ over the visible frequencies range (*5*), that is, the behavior expected for ideal Dirac fermions.

The agreement between the experiment and theory is striking because it was believed that the universality could hold only for low energies ($E < 1$ eV), beyond which the electronic spectrum of graphene becomes strongly warped and nonlinear and the approximation of Dirac fermions breaks down. However, our calculations (*5*) show that finite-E corrections are surprisingly small (a few %) even for visible light. Because of these corrections, a metrological accuracy for α would be difficult to achieve, but it is remarkable that the fine structure constant can so directly be assessed practically by the naked eye.

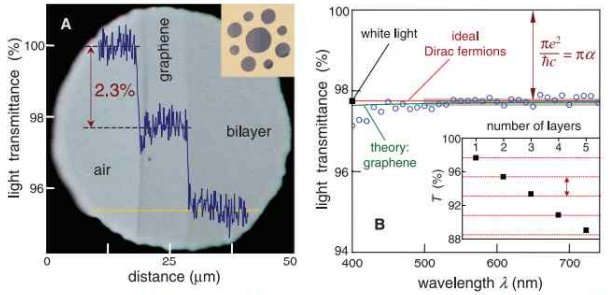

Fig. 1. Looking through one-atom-thick crystals. **(A)** Photograph of a 50-μm aperture partially covered by graphene and its bilayer. The line scan profile shows the intensity of transmitted white light along the yellow line. (Inset) Our sample design: A 20-μm-thick metal support structure has several apertures of 20, 30, and 50 μm in diameter with graphene crystallites placed over them. **(B)** Transmittance spectrum of single-layer graphene (open circles). Slightly lower transmittance for $\lambda < 500$ nm is probably due to hydrocarbon contamination (*5*). The red line is the transmittance $T = (1 + 0.5\pi\alpha)^{-2}$ expected for two-dimensional Dirac fermions, whereas the green curve takes into account a nonlinearity and triangular warping of graphene's electronic spectrum. The gray area indicates the standard error for our measurements (*5*). (Inset) Transmittance of white light as a function of the number of graphene layers (squares). The dashed lines correspond to an intensity reduction by $\pi\alpha$ with each added layer.

References and Notes

1. A. K. Geim, K. S. Novoselov, *Nat. Mater.* **6**, 183 (2007).
2. T. Ando, Y. Zheng, H. Suzuura, *J. Phys. Soc. Jpn.* **71**, 1318 (2002).
3. V. P. Gusynin, S. G. Sharapov, J. P. Carbotte, *Phys. Rev. Lett.* **96**, 256802 (2006).
4. A. B. Kuzmenko, E. van Heumen, F. Carbone, D. van der Marel, *Phys. Rev. Lett.* **100**, 117401 (2008).
5. Materials and methods are available on *Science* Online.
6. J. S. Bunch *et al.*, *Science* **315**, 490 (2007).

7. We are grateful to A. Kuzmenko, A. Castro Neto, P. Kim, and L. Eaves for illuminating discussions. Supported by Engineering and Physical Sciences Research Council (UK), the Royal Society, European Science Foundation, and Office of Naval Research.

Supporting Online Material

www.sciencemag.org/cgi/content/full/1156965/DC1
Materials and Methods
SOM Text
Figs. S1 to S5
References

25 February 2008; accepted 26 March 2008
Published online 3 April 2008;
10.1126/science.1156965
Include this information when citing this paper.

[1]Manchester Centre for Mesoscience and Nanotechnology, University of Manchester, M13 9PL Manchester, UK. [2]Department of Physics, University of Minho, P-4710-057 Braga, Portugal.
*To whom correspondence should be addressed. E-mail: geim@man.ac.uk

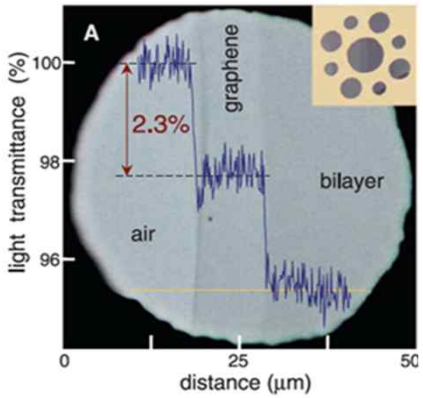

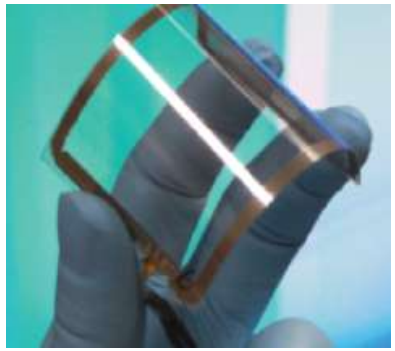

The opacity of suspended graphene is defined solely by the fine structure constant, $\alpha = e^2/hc = 1/137$ (where c is the speed of light), the parameter that describes coupling between light and relativistic electrons and that is traditionally associated with quantum electrodynamics rather than materials science. Despite being only one atom thick, graphene is found to absorb a significant ($\pi\alpha = 2.3\%$) fraction of incident white light, a consequence of graphene's unique electronic structure.

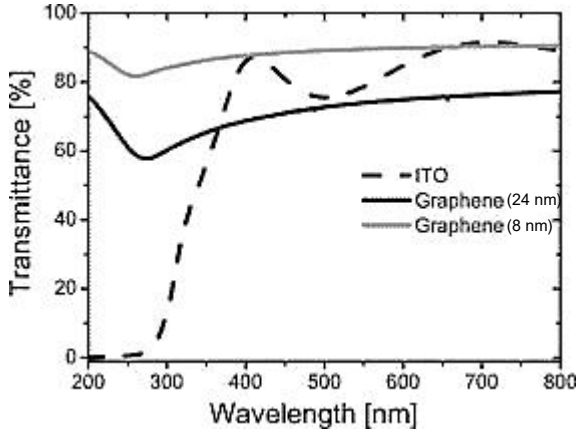

R. R. Nair et al. Science (2008)
C. M. Weber et al. Small (2009)

Interband Absorption in Graphene

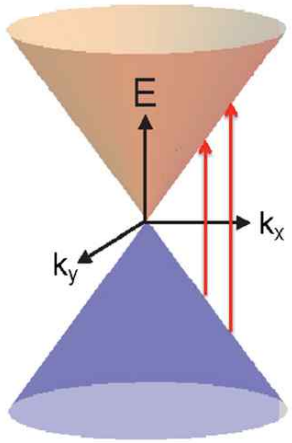

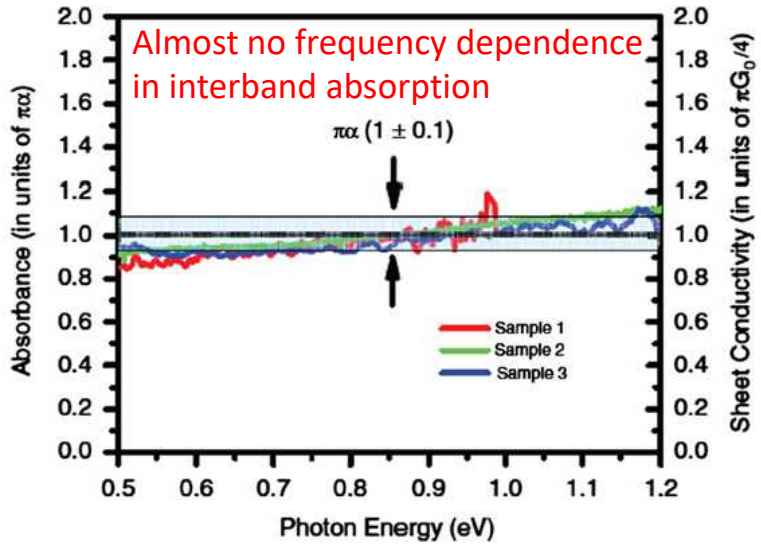

Tunable absorption by doping

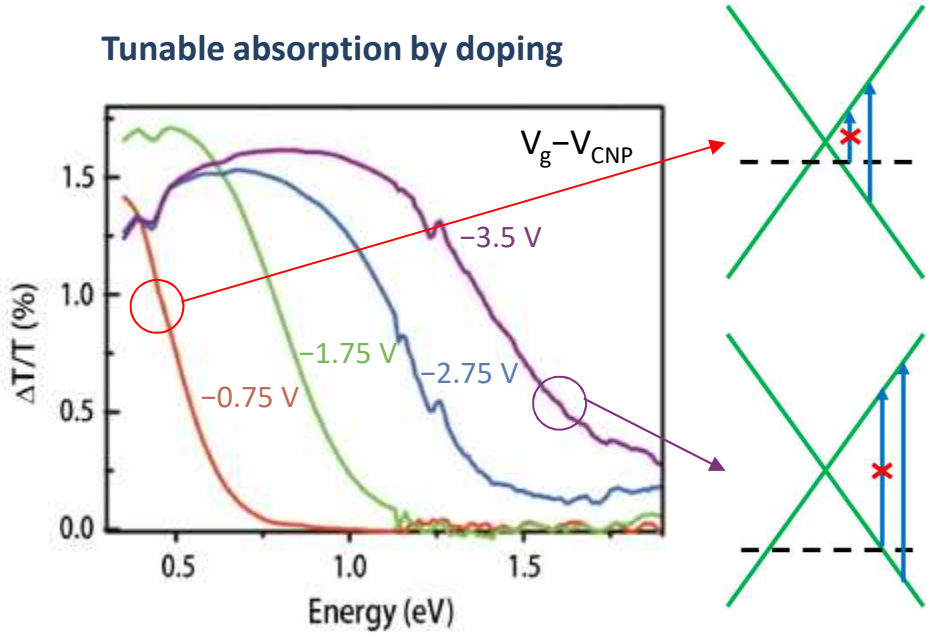

K. F. Mak Solid State Commun. 152, 1341-1349 (2012)

Optical Properties of Graphene

Graphene quantum dots

Fabrication

Top-down method
: nanolithography, acidic oxidation, hydrothermal, etc.

Bottom-up method
: stepwise solution chemistry, microwave-assisted, etc.

GQD size
: 3-20nm (<5L)

Shape
: circular, elliptical, triangular, quadrate, hexagonal

Surface group
: Modification of optical structure

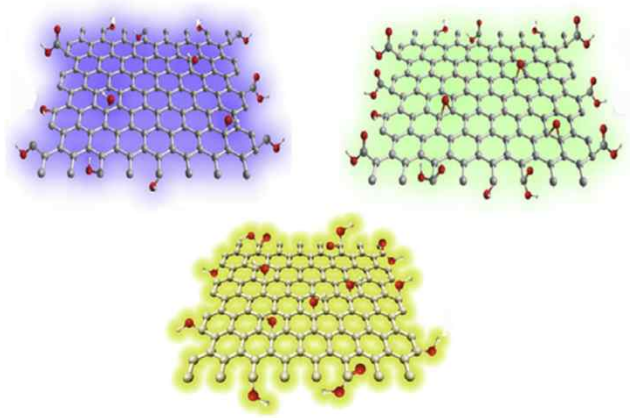

H. Sun et al. Mater. Today (2013)

Graphene Quantum Dots (GQDs)

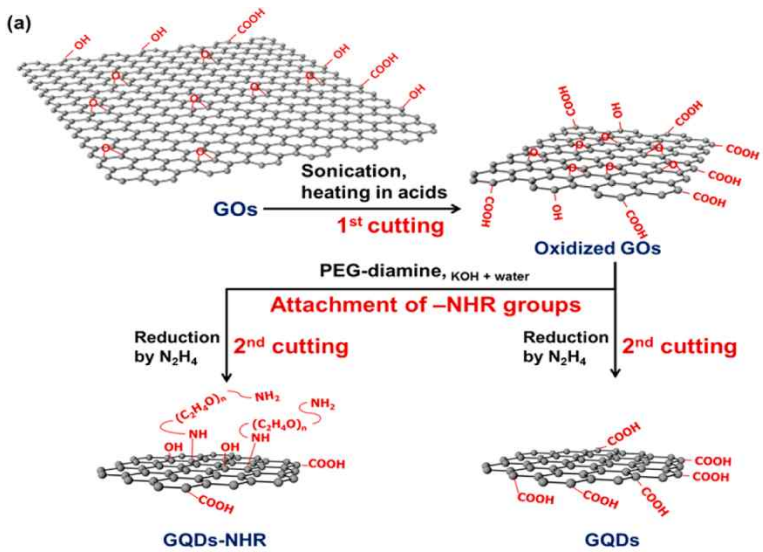

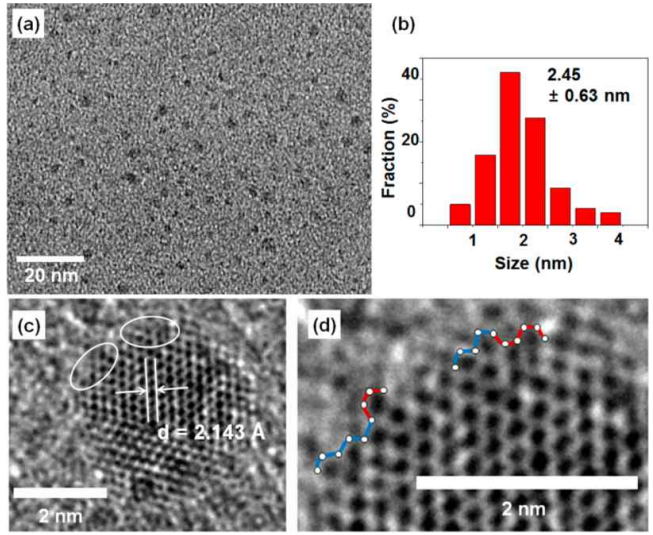

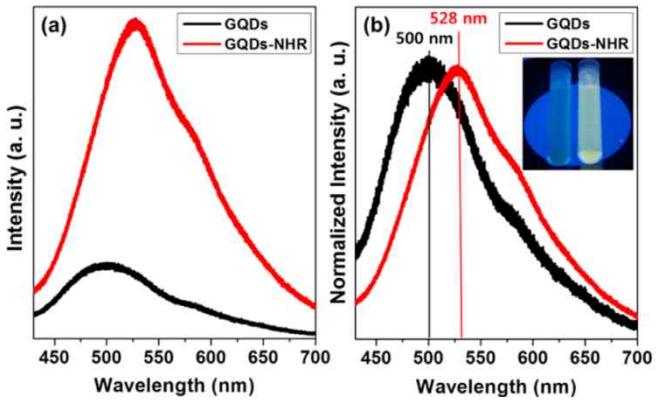

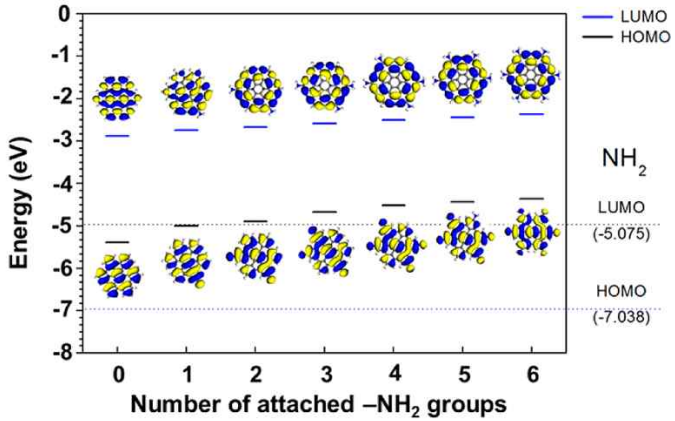

- PL control of GQDs by adjusting size and adding functional groups at edges.

S. H. Jin et al. ACS Nano (2013)

Mechanical Properties of Graphene

Measurement of stiffness and strength of graphene

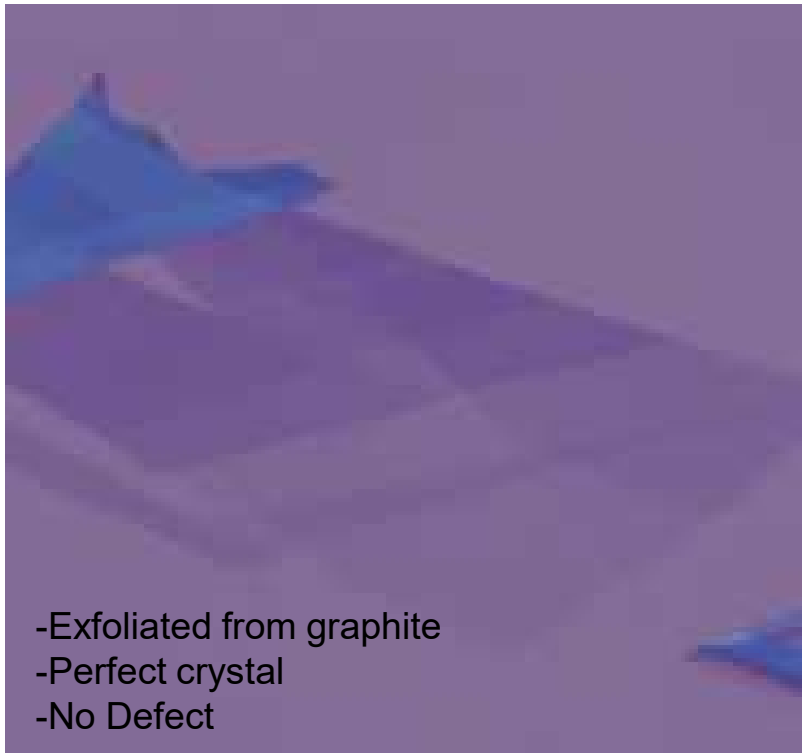

E=340 N m^{-1} (E_{3D} = 1 TPa)
σ=42 N m^{-1} (σ_{3D} = 130 GPa)

AFM and Nanoindenter

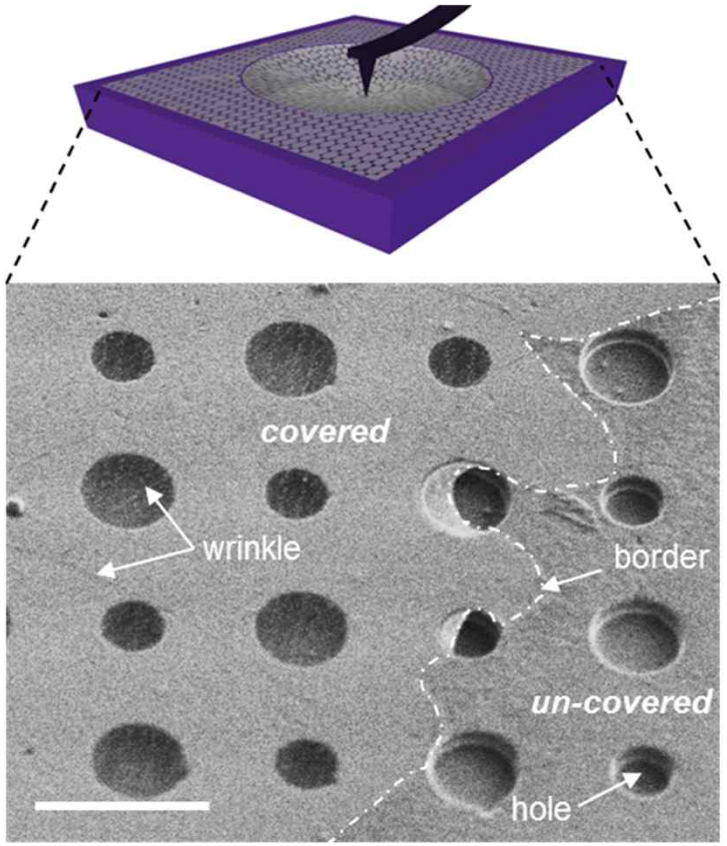

C. Lee et al. Science (2008)

Mechanical Properties of Graphene Grain Boundary

Structure of CVD Graphene

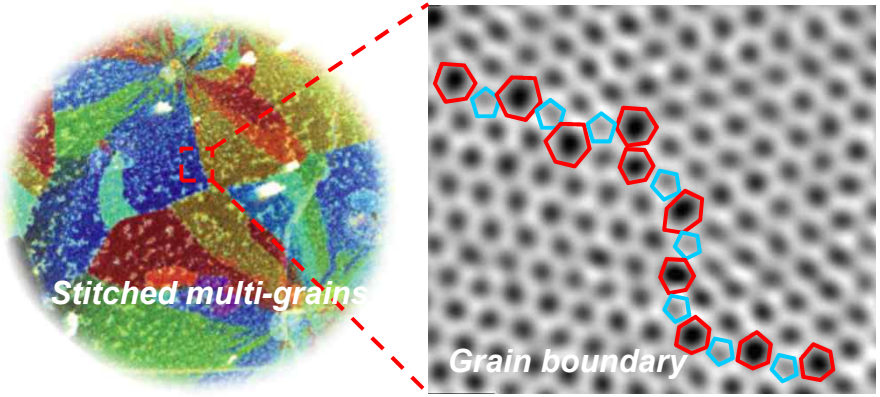

P. Y. Huang et al, Nature (2011)

Strength Measurement of Grain Boundary

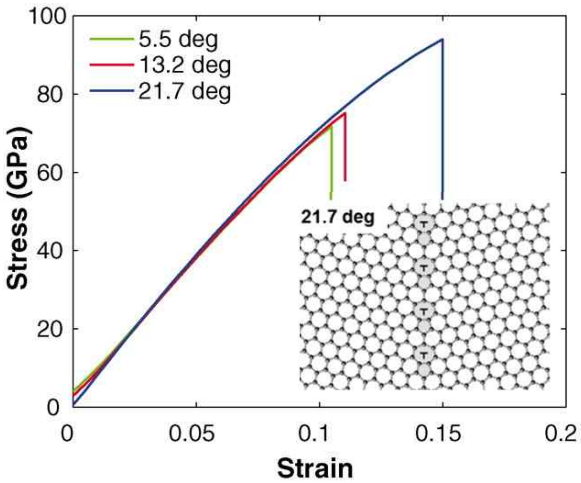

R. Grantab et al, Science (2010)

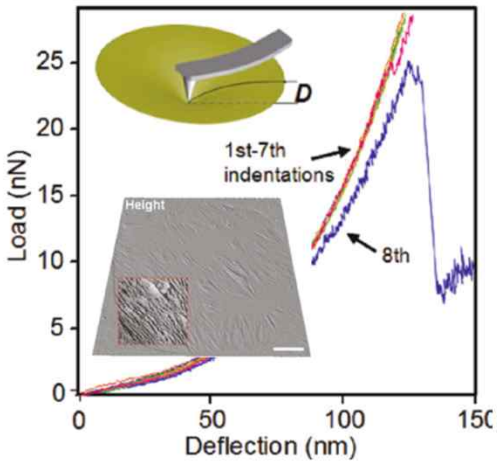

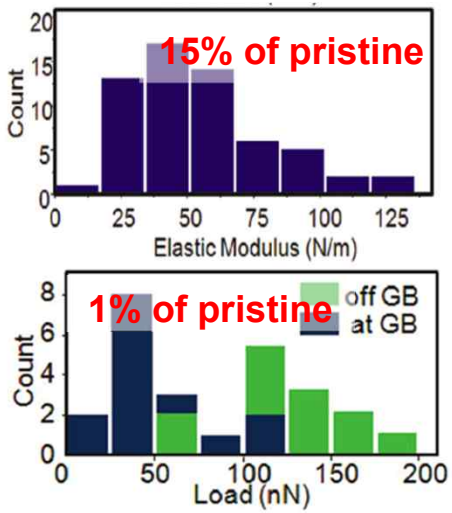

C. S. Ruiz-Vargas et al. Nano Lett (2011)

Growth Control of Graphene

Small Grain Graphene (SG)

- Pressure: 300 mTorr
- Flow rate: 35 sccm methane
- Directly exposed on copper foil

→ *multi-grain graphene with 1-5μm size*

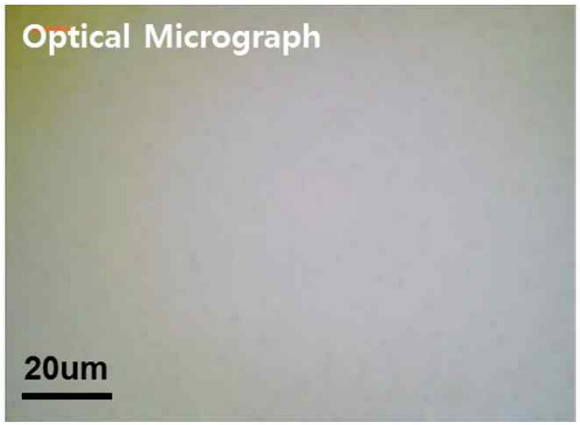

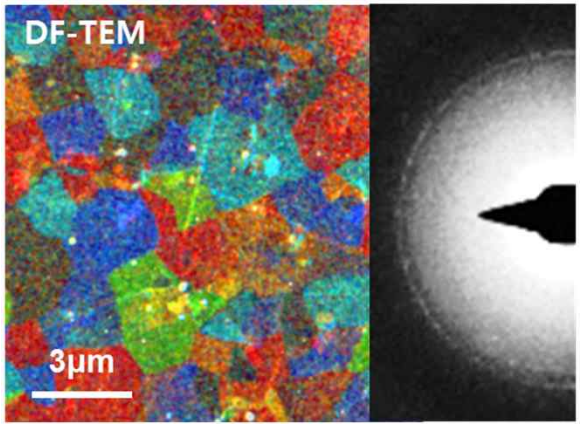

Large Grain Graphene (LG)

- Pressure: <50 mTorr
- Flow rate: 1 sccm Methane
- Enclosed copper foil (by Ruoff group)

→ *single-grain graphene with 100-150μm*

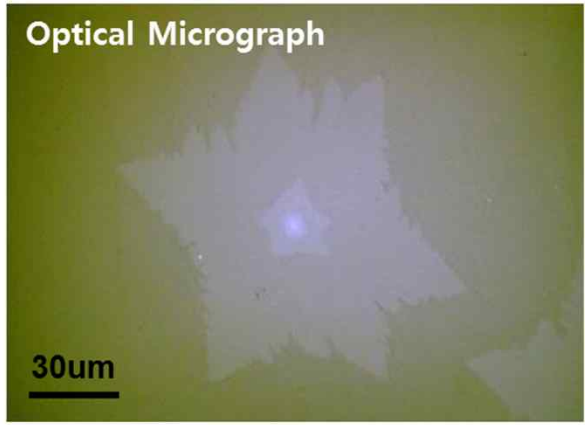

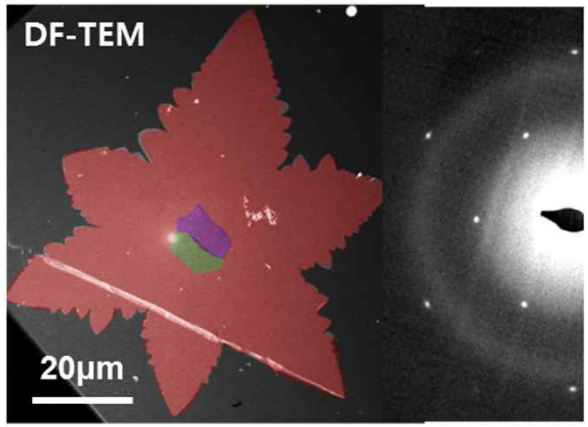

G.H. Lee, J. Hone ***Science*** *(2013)*

Sample Preparation for Nano-indentation

Dry Transfer Process

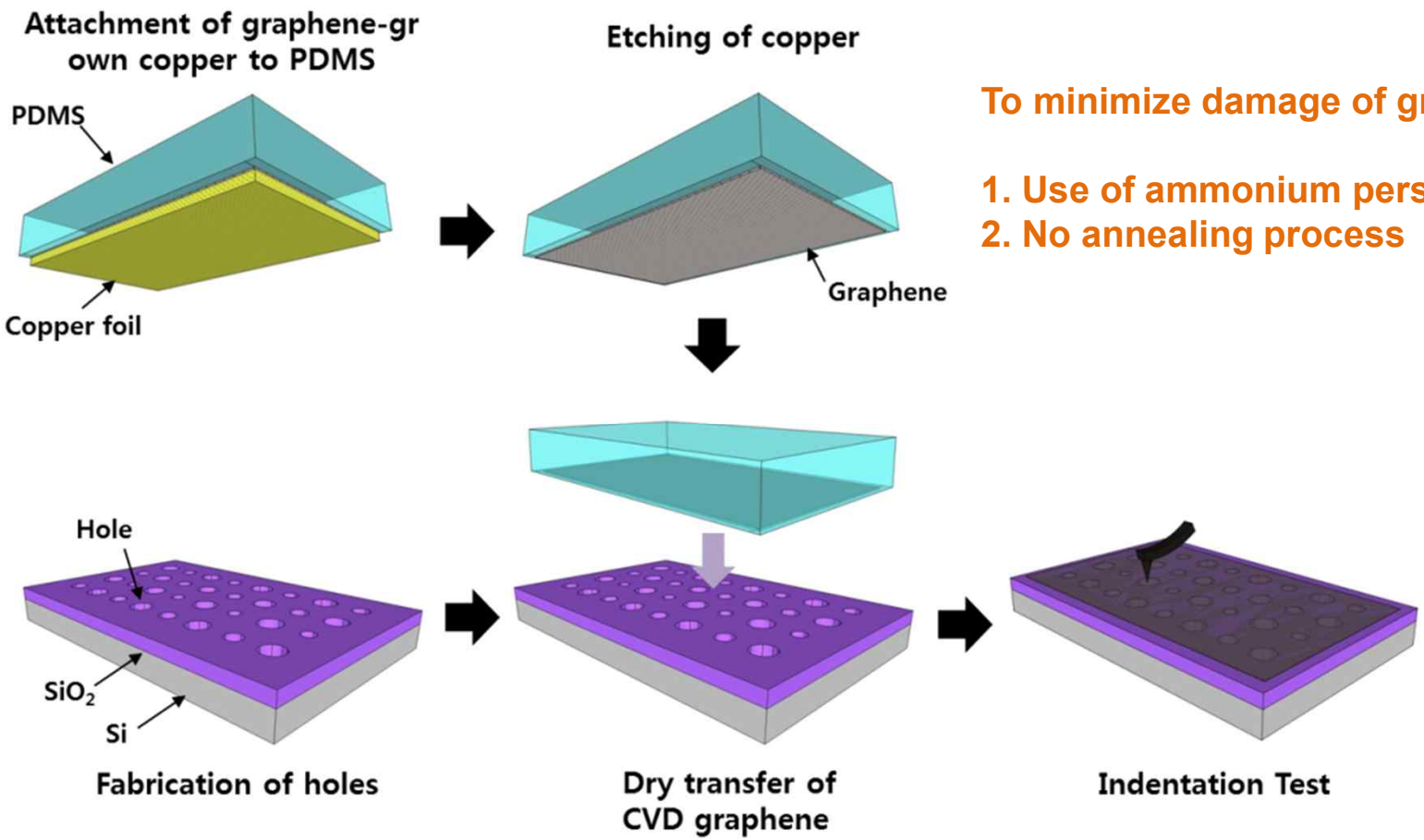

To minimize damage of graphene

1. Use of ammonium persulfate
2. No annealing process

G.H. Lee, J. Hone ***Science*** *(2013)*

Nano-indentation

AFM and Nanoindenter

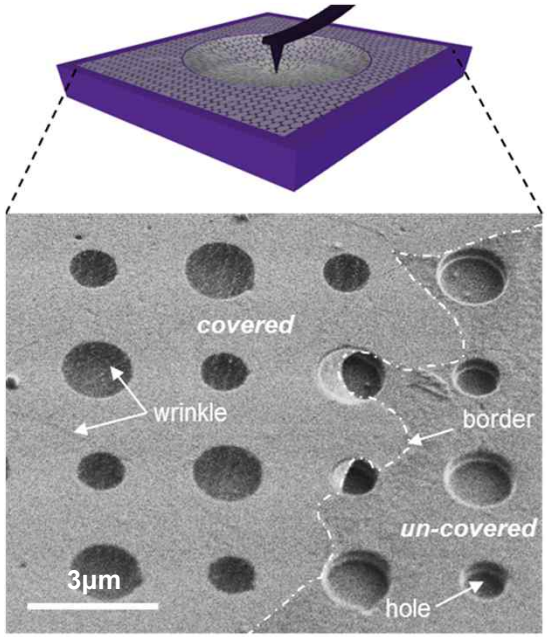

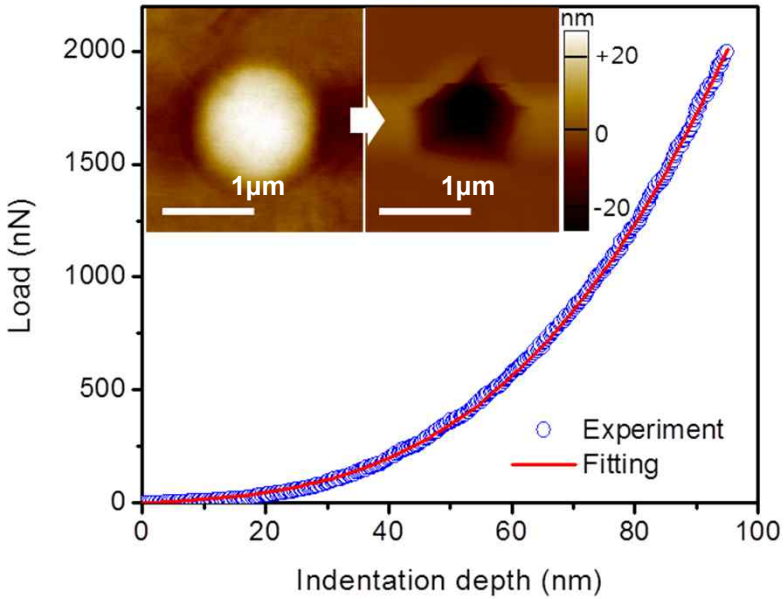

Semi-empirical relationship

$$F \approx \sigma_0^{2D}(\pi a)\left(\frac{\delta}{a}\right) + E^{2D}\left(q^3 a\right)\left(\frac{\delta}{a}\right)^3$$

σ_0^{2D} = 2D pre-tension (N m^{-1})

E^{2D} = 2D stiffness (N m^{-1})

G.H. Lee, J. Hone ***Science*** *(2013)*

Statistical Analyses of Mechanical Properties

Elastic Stiffness

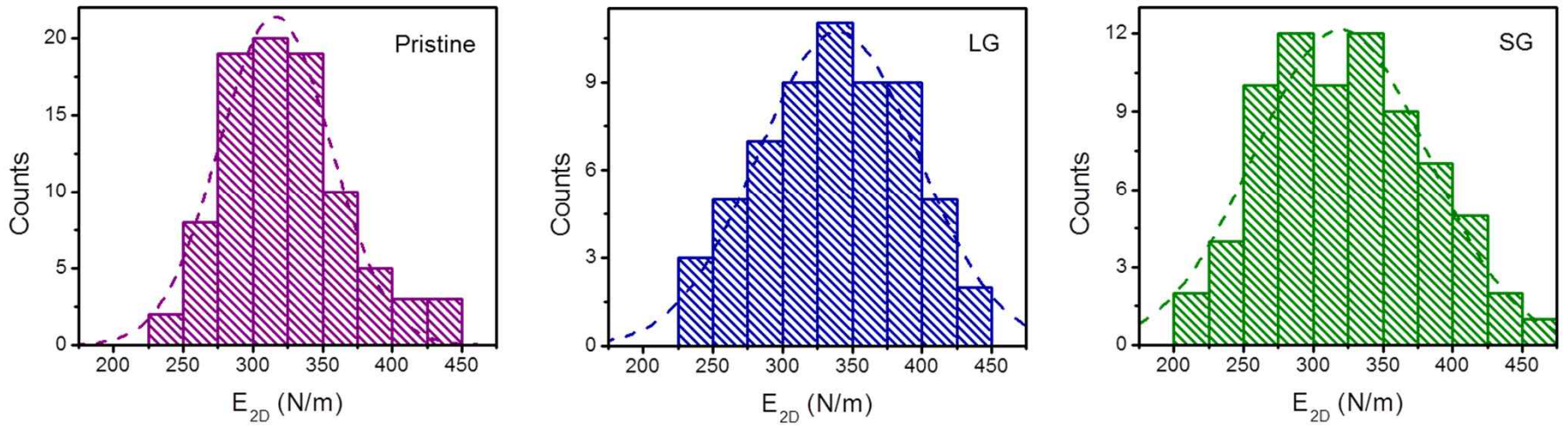

Fracture Load

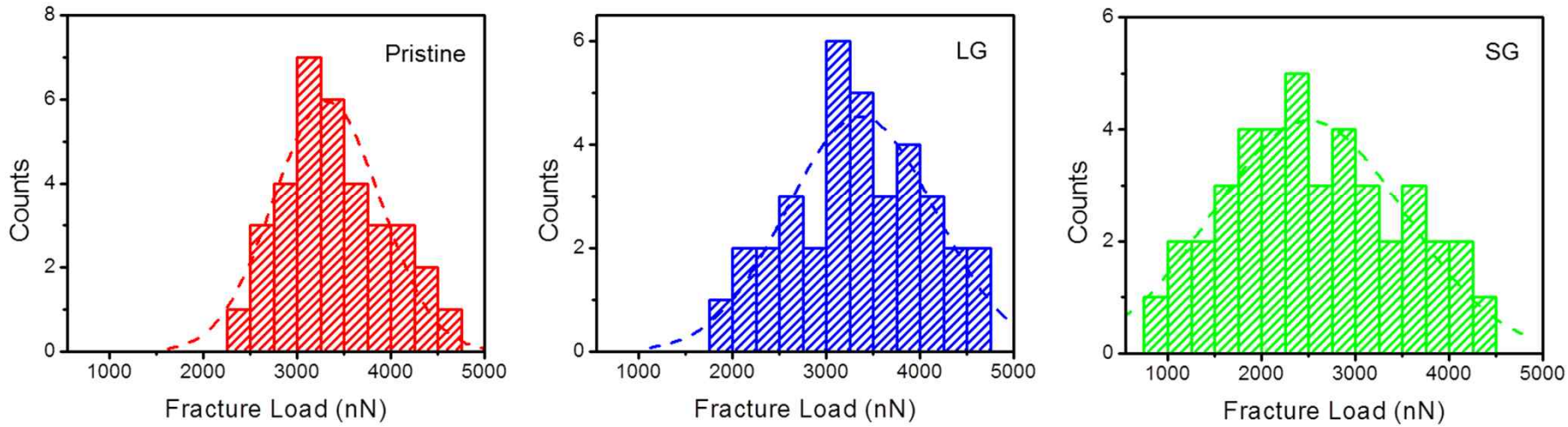

G.H. Lee, J. Hone ***Science*** *(2013)*

Non-Linear Elasticity of Graphene

Strain energy density as a Taylor series in powers of strain

$$\Phi = \frac{1}{2!}C_{ijkl}\eta_{ij}\eta_{kl} + \frac{1}{3!}C_{ijklmn}\eta_{ij}\eta_{kl}\eta_{mn} + \frac{1}{4!}C_{ijklmnop}\eta_{ij}\eta_{kl}\eta_{mn}\eta_{op} + \frac{1}{5!}C_{ijklmnopqr}\eta_{ij}\eta_{kl}\eta_{mn}\eta_{op}\eta_{qr}$$

Second Piola-Kirchhoff Stress

$$\Sigma_{ij} = \frac{\partial\Phi}{\partial\eta_{ij}} = C_{ijkl}\eta_{kl} + \frac{1}{2!}C_{ijklmn}\eta_{kl}\eta_{mn} + \frac{1}{3!}C_{ijklmnop}\eta_{kl}\eta_{mn}\eta_{op} + \frac{1}{4!}C_{ijklmnopqr}\eta_{kl}\eta_{mn}\eta_{op}\eta_{qr}\cdots$$

5th-order non-linear continuum formulation fit to DFT calculations

Finite element method (FEM)

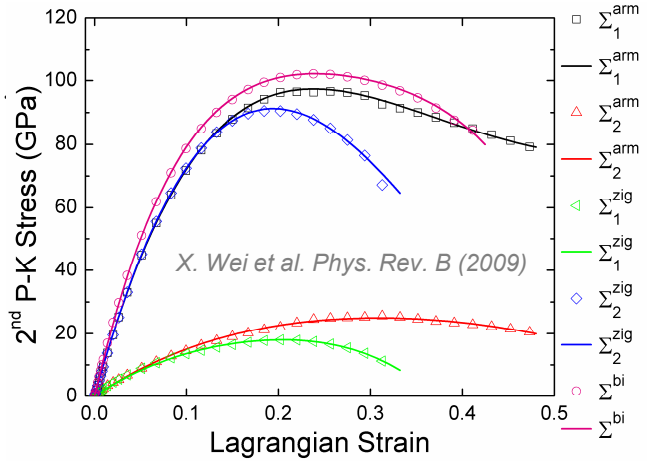

Stress vs. Load

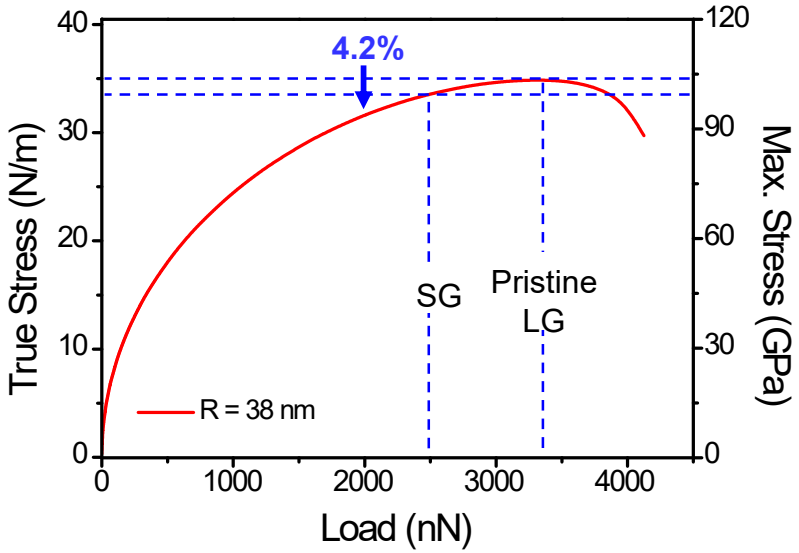

Stress vs. Strain

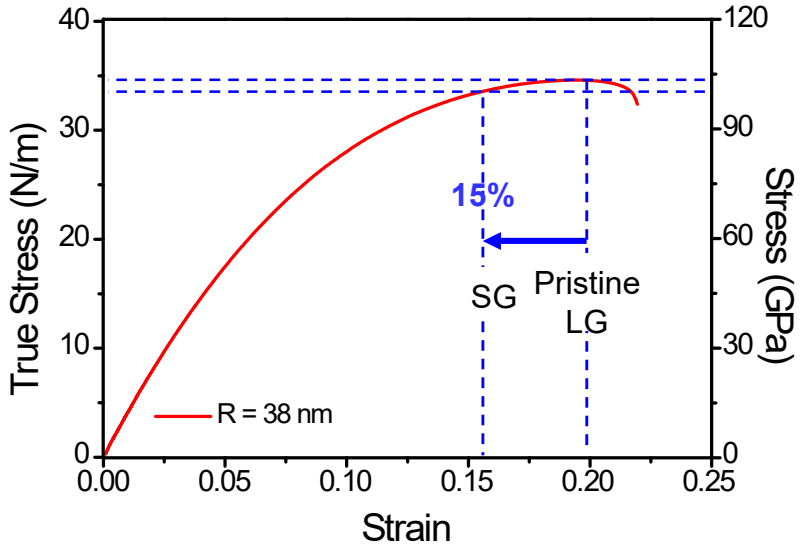

Large-grain graphene sheet without grain boundaries is as strong as pristine graphene. Furthermore, polycrystalline graphene with grain boundaries can also act as a large-area ultrastrong material.

G.H. Lee, J. Hone ***Science*** *(2013)*

Strength of Grain Boundary

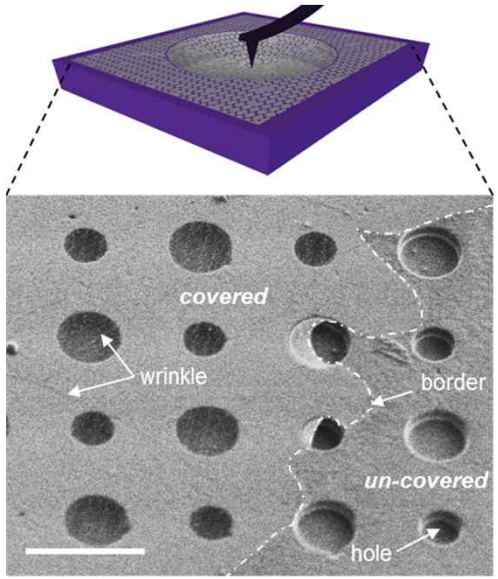

Direct Indentation on Grain Boundary

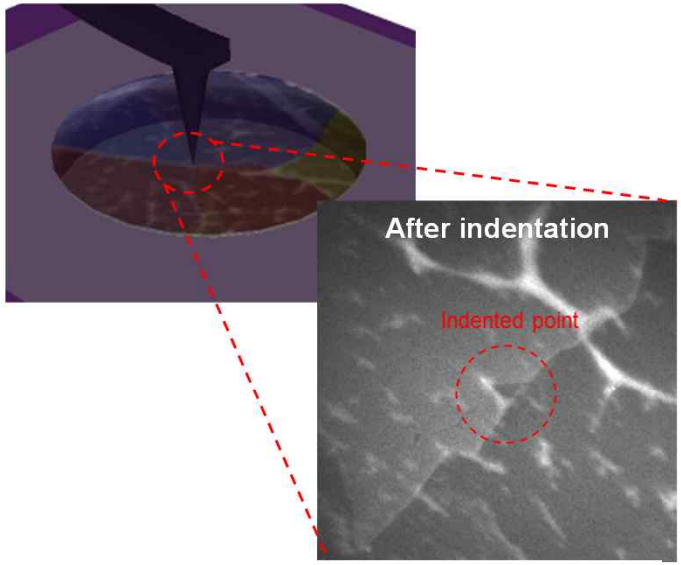

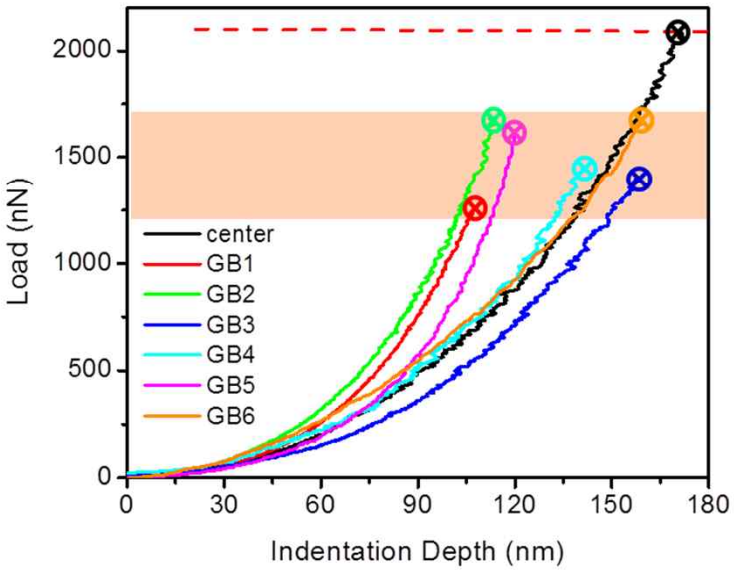

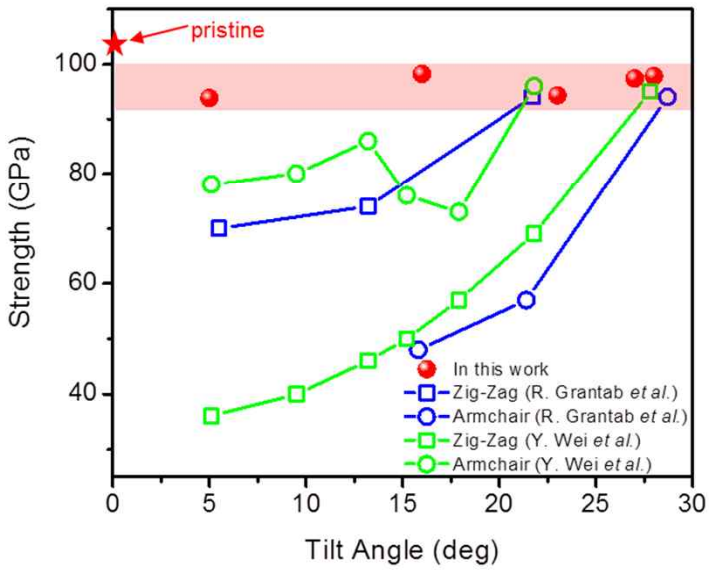

Simulation

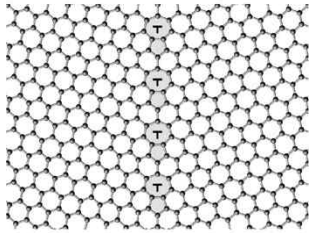

Realistic

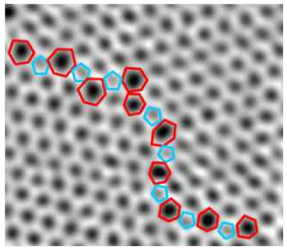

G.H. Lee, J. Hone ***Science*** *(2013)*

Is Graphene Practically Strong?

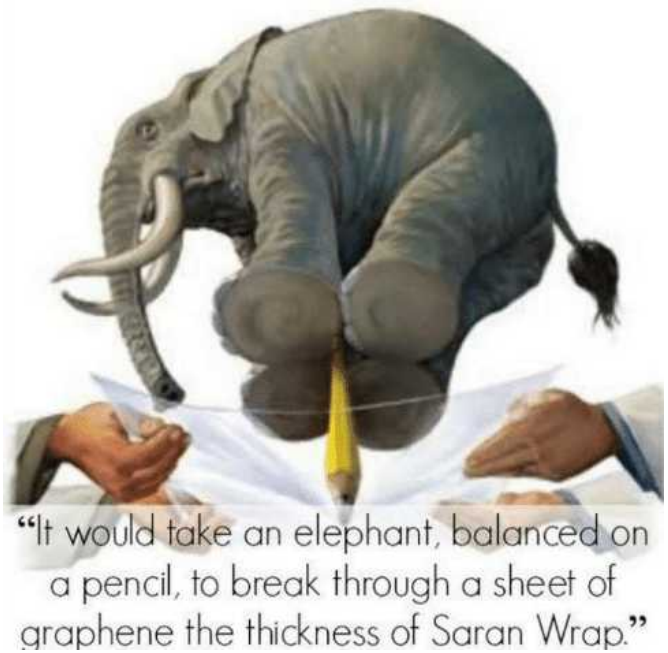

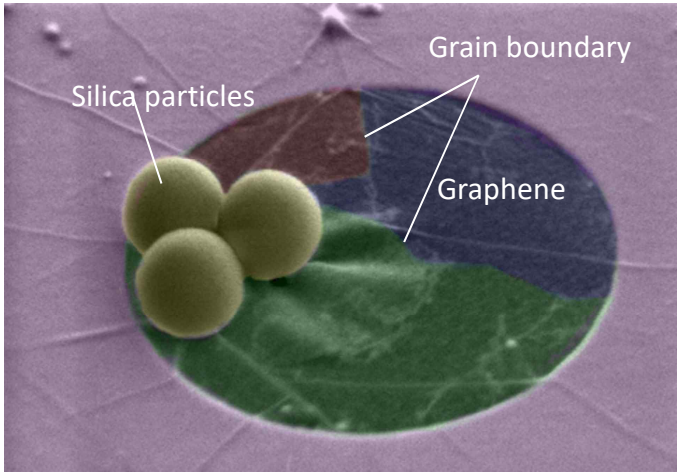

In real world

In nano world

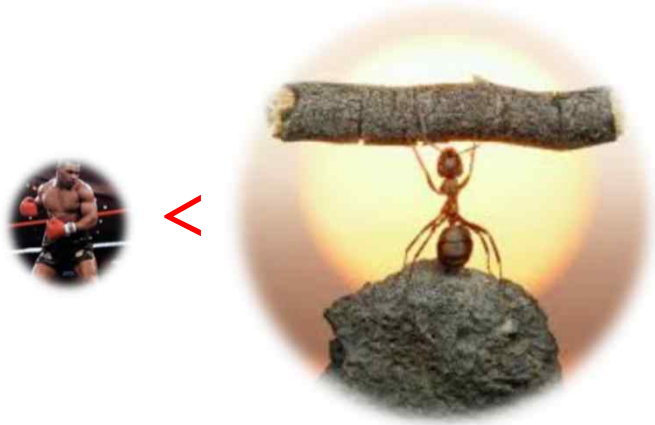

Graphene Bulletproof vest

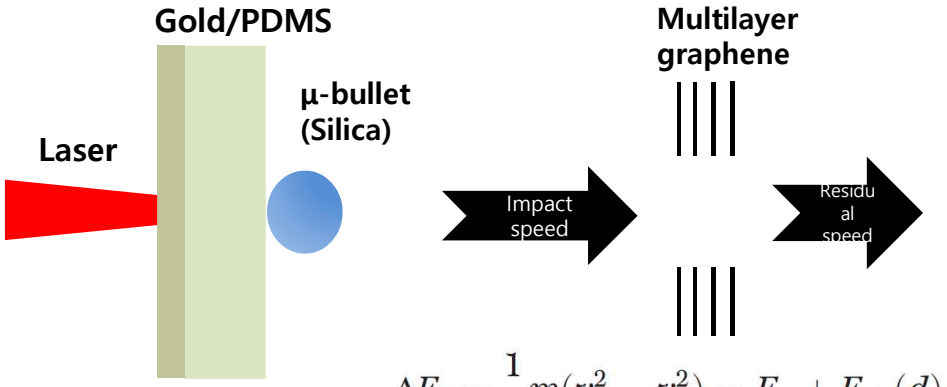

$$\Delta E_k = \frac{1}{2} m(v_i^2 - v_r^2) = E_p + E_{air}(d)$$

E_p : *penetration energy*

E_{air} : *energy loss due to air drag*

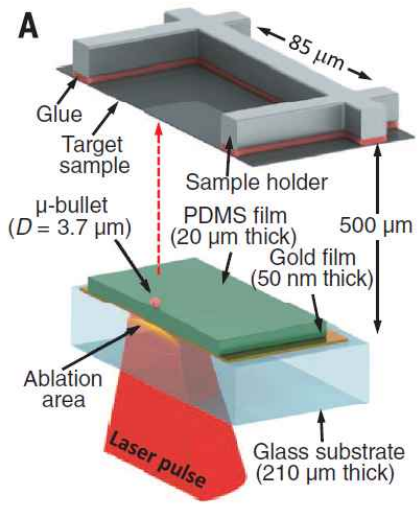

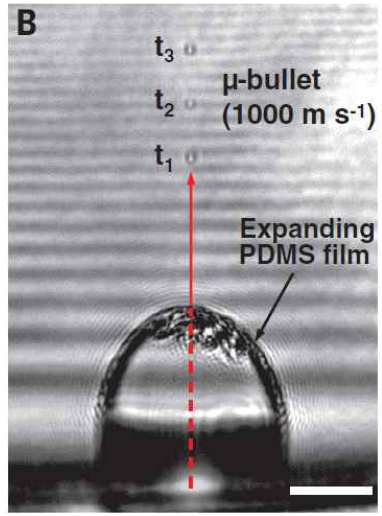

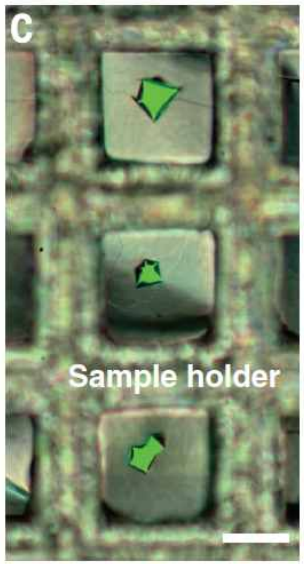

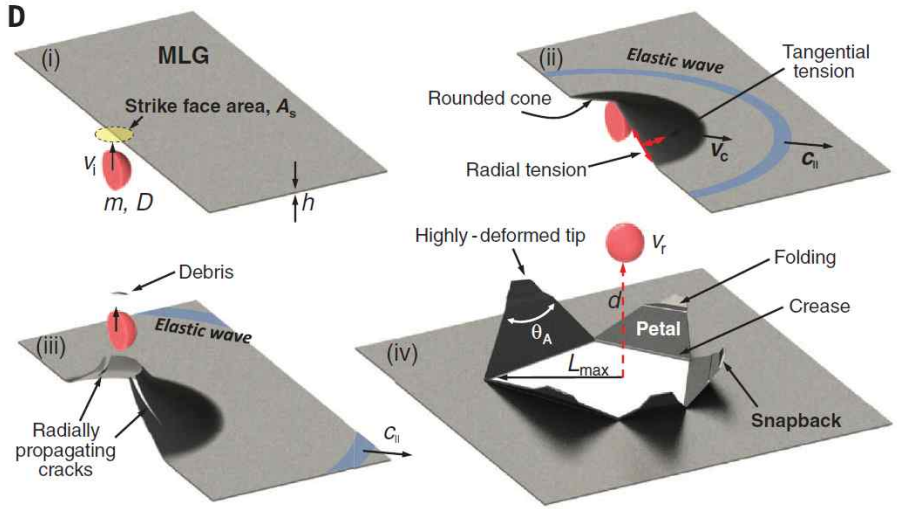

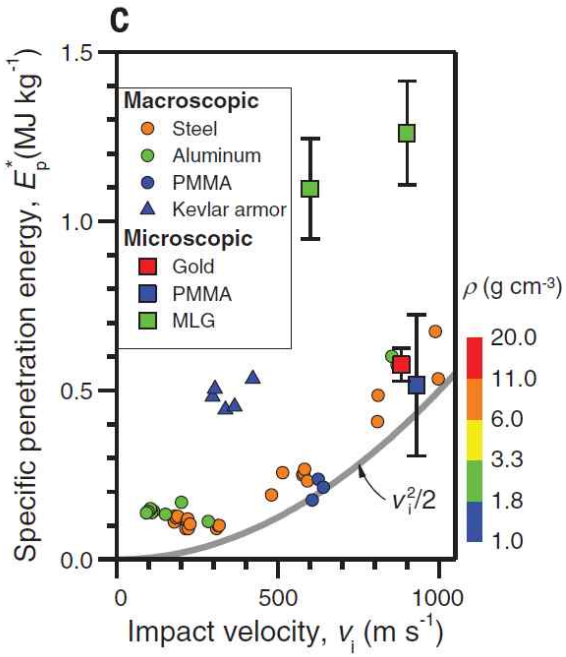

Graphene has 8~12 times higher specific penetration energy than steel.

J. H. Lee et al. Science (2014)

Mechanical Properties of Graphene

Fatigue test

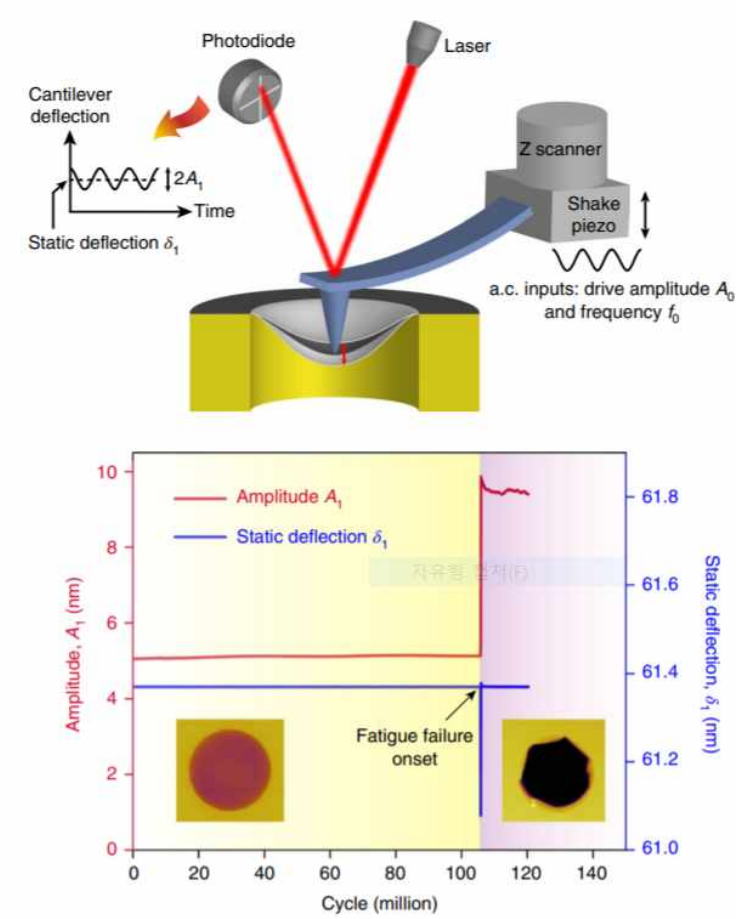

T. Cui et al. Nature Materials (2020)

Elastic straining test

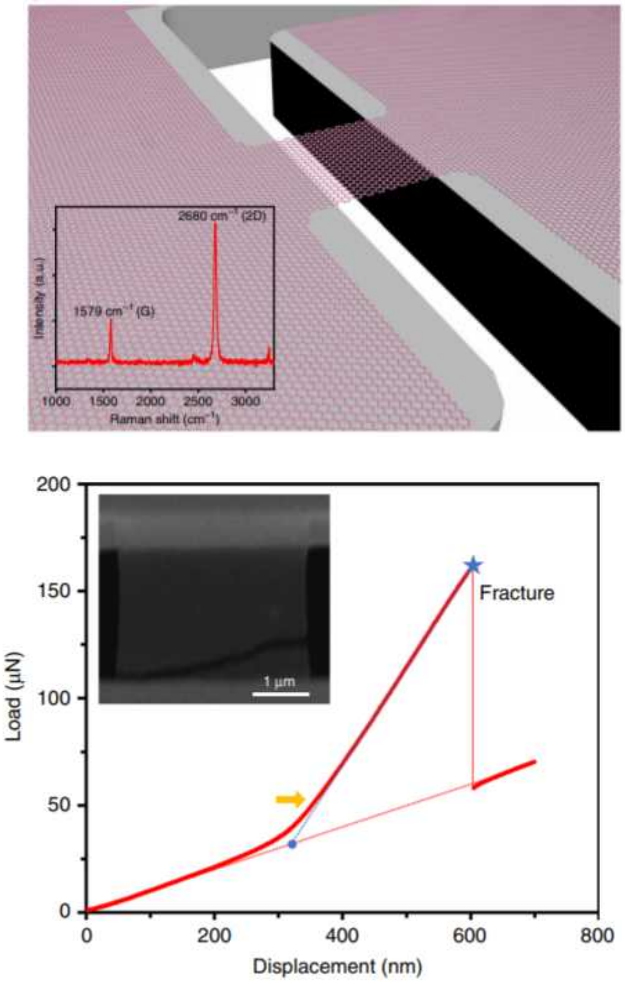

Nature Comm. 11, 284 (2020)

Diamene

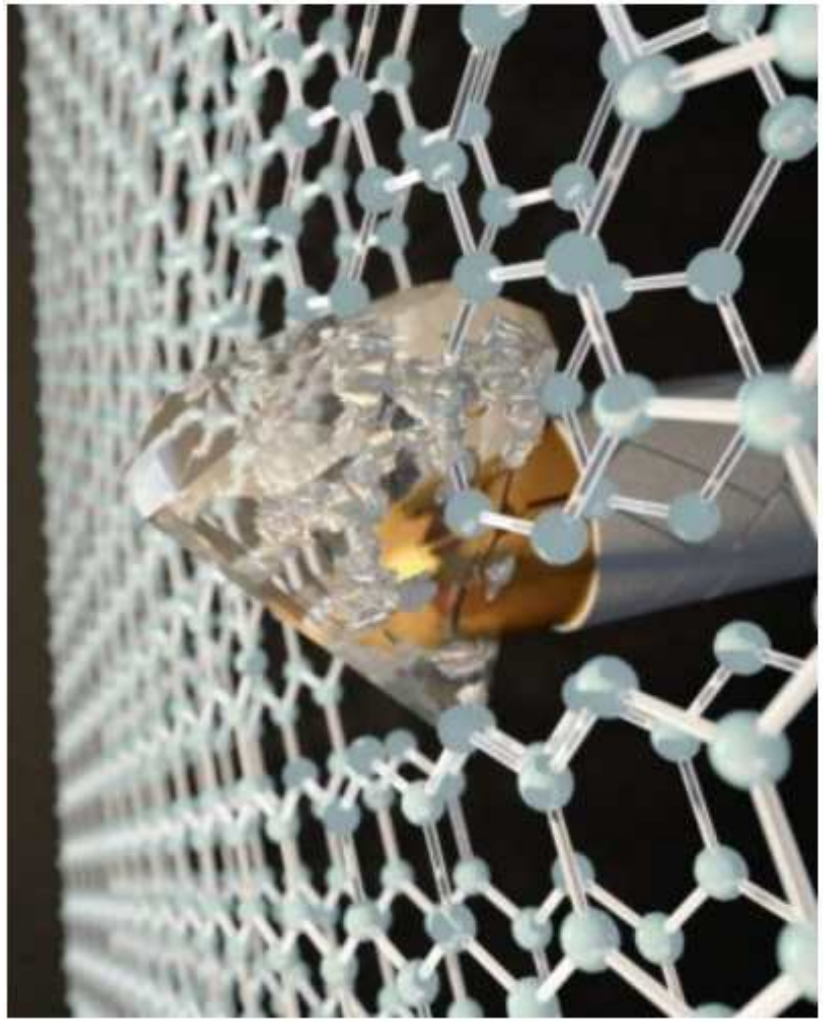

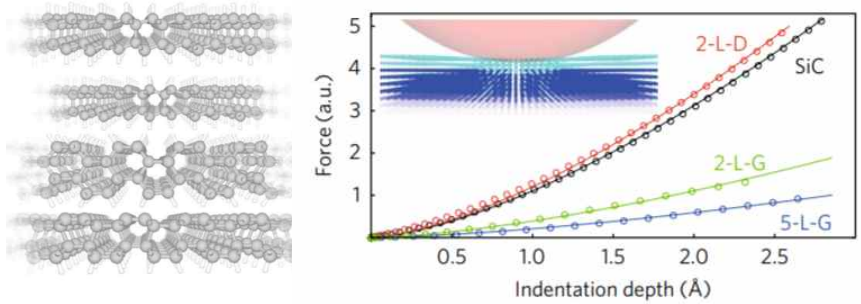

Nanotechnology 13 (2), 133–138. (2017)

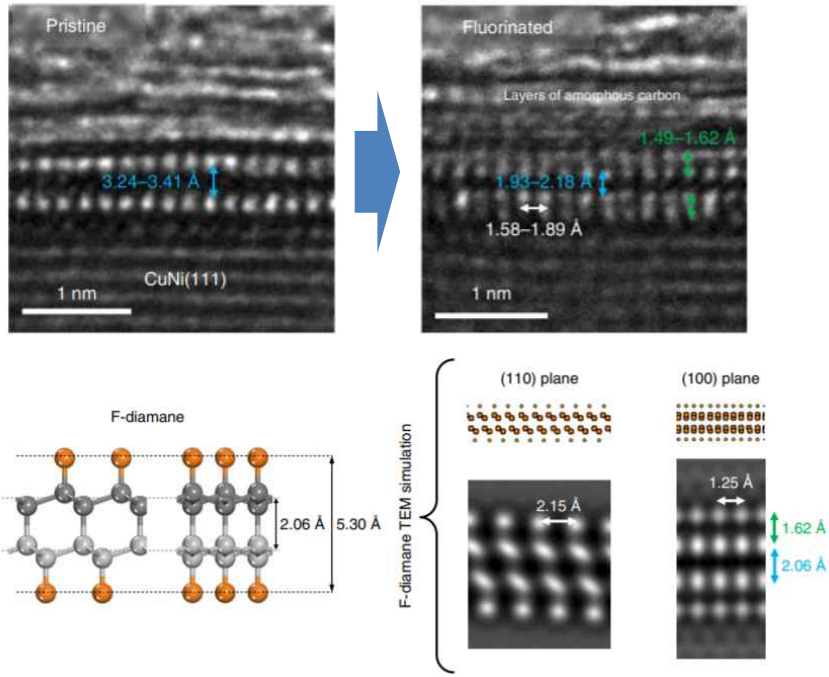

Nature Nanotechnology 15, 59–66 (2020)

Chemical and Bio Properties of Graphene

3D structure

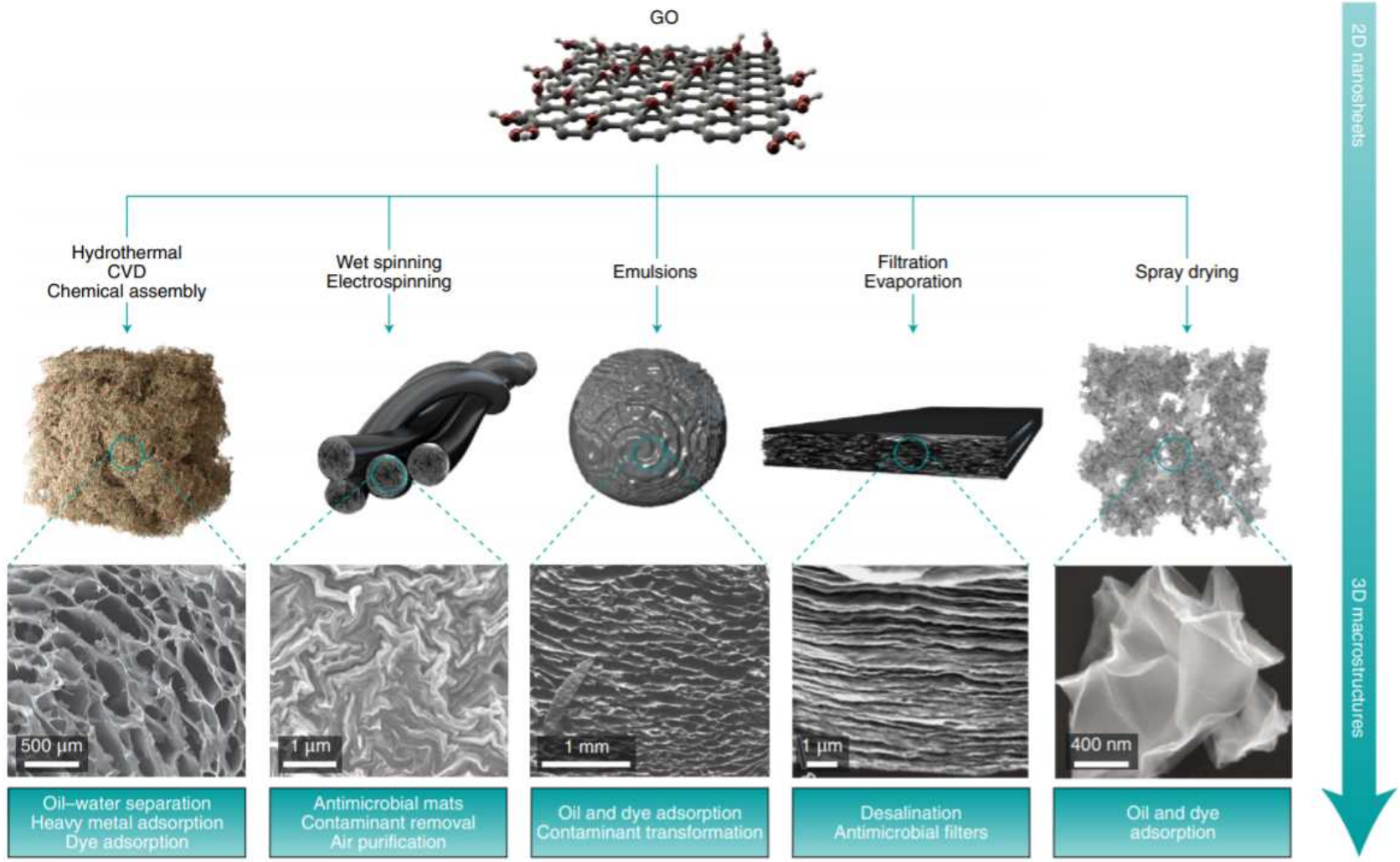

Nature Nanotechnology 14, 107–119 (2019)

Chemical and Bio Properties of Graphene

Bio application

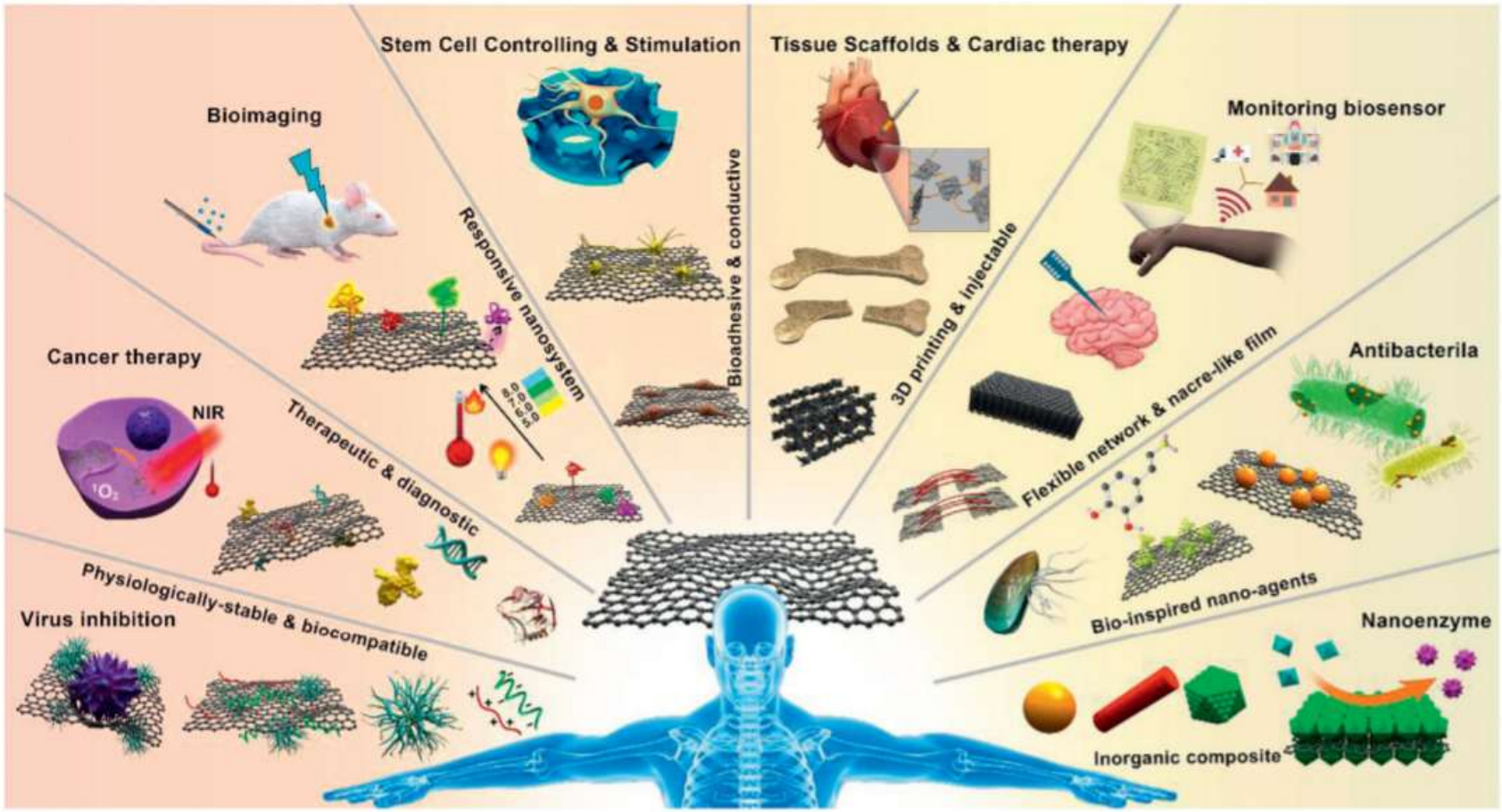

Nano Today 26, 57–97 (2019)

Chemical and Bio Properties of Graphene

Bio-favorable substrate

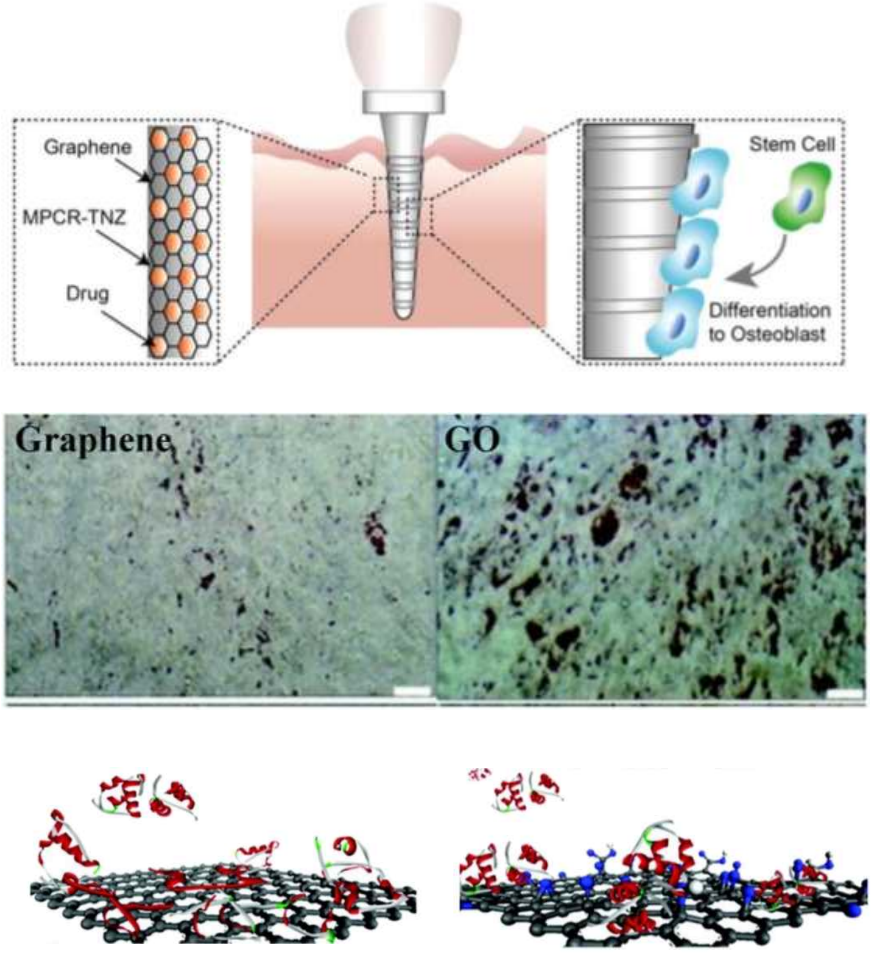

Communications Chemistry 3, 8 (2020)

3D printing

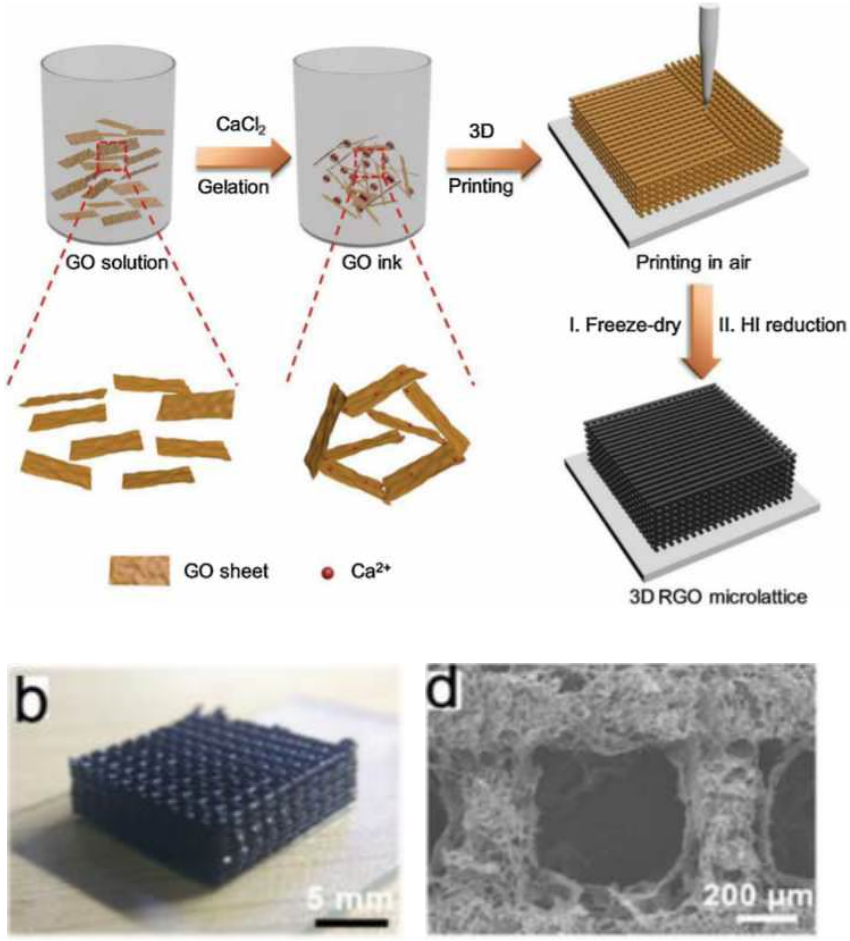

Nano Today 26, 57–97 (2019)